

On the importance of multiphase photolysis of organic nitrates on their global atmospheric removal

Juan Miguel González-Sánchez^{1,2}, Nicolas Brun^{1,2}, Junteng Wu¹, Sylvain Ravier¹, Jean-Louis Clément², Anne Monod¹

5 ¹Aix Marseille Univ, CNRS, LCE, Marseille, France

²Aix Marseille Univ, CNRS, ICR, Marseille, France

Correspondence to: Juan Miguel González-Sánchez (juan.gonzalez@mio.osupytheas.fr) and Anne Monod (anne.monod@univ-amu.fr)

10 **Abstract.** Organic nitrates (RONO₂) are secondary compounds, and their fate is related to the transport and removal of NO_x in the atmosphere. While previous research studies have focused on the reactivity of these molecules in the gas phase, their reactivity in condensed phases remains poorly explored despite their ubiquitous presence in submicron aerosol. This work investigated for the first time the aqueous-phase photolysis rate constants and quantum yields of four RONO₂ (isopropyl nitrate, isobutyl nitrate, α -nitrooxyacetone, and 1-nitrooxy-2-propanol). Our results showed much lower photolysis rate constants for
15 these RONO₂ in the aqueous phase than in the gas phase. From alkyl nitrates to polyfunctional RONO₂, no significant increase of their aqueous-phase photolysis rate constants was observed, even for RONO₂ with conjugated carbonyl groups, in contrast with the corresponding gas-phase photolysis reactions. Using these new results, extrapolated to other alkyl and polyfunctional RONO₂, in combination with estimates for the other atmospheric sinks (hydrolysis, gas phase photolysis, aqueous and gas phase \cdot OH oxidation, dry and wet deposition) multiphase atmospheric lifetimes were calculated for 45 atmospherically relevant
20 RONO₂ along with the relative importance of each sink. Their lifetimes range from a few minutes to several hours depending on the RONO₂ chemical structure and its water solubility. In general, multiphase atmospheric lifetimes are lengthened when RONO₂ partition to the aqueous phase, especially for conjugated carbonyl nitrates for which lifetimes can increase by up to 100 %. Furthermore, our results show that aqueous-phase \cdot OH oxidation is a major sink for water-soluble RONO₂ ($K_H > 10^5$ M atm⁻¹) ranging from 50 to 70 % of their total sink at high LWC (0.35 g m⁻³). These results highlight the importance of
25 investigating the aqueous-phase RONO₂ reactivity to understand how it affects their ability to transport air pollution.

1 Introduction

Organic nitrates play a key role in the formation, transport, and removal of NO_x. They are secondary compounds formed *via* NO_x + VOC reactions. Depending on their structure, their lifetimes can be long (from a couple of hours to several days) thus they can be transported from polluted areas where they are formed to more remote areas (Shepson, 1999). During their long-
30 range transport, these molecules are subject to reactions (i.e.: gas-phase photolysis and/or \cdot OH oxidation) releasing back NO_x.

RONO₂ are thus responsible for homogenizing the distribution of NO_x and consequently, they impact other major pollutants such as O₃ and secondary organic aerosol (SOA) (Perring et al., 2013). Besides, RONO₂ can remove NO_x from the atmosphere by deposition to the Earth's surface or by transformation into a more inert chemical compound such as nitric acid (Hu et al., 2011; Nguyen et al., 2015). Therefore, their atmospheric reactivity and fate must be considered to accurately predict the transport of pollution on a regional scale. Besides, this is of special importance for world regions with decreasing NO_x levels (such as Europe and North America) where the RONO₂ relative importance as NO_x reservoir and sink is increasing due to an increase in the overall rate of transformation of NO_x to RONO₂ (Romer Present et al., 2020).

Numerous studies have investigated the gas-phase reactivity of individual RONO₂ molecules (Suarez-Bertoa et al., 2012; Picquet-Varrault et al., 2020; Bedjanian et al., 2018; Talukdar et al., 1997a, b; Clemitshaw et al., 1997; Atkinson and Aschmann, 1989; Morin et al., 2016), mainly focusing on ·OH-oxidation and photolysis. Their results show that the kinetics and mechanisms of these reactions are highly influenced by the RONO₂ chemical structure. Although the presence of the nitrate group in the molecule hinders the ·OH attack, ·OH-oxidation generally represents the main RONO₂ gas-phase sink (Shepson, 1999). However, RONO₂ with conjugated carbonyl groups are consumed faster *via* photolysis due to an enhancement in their light absorption. This is of high importance for ubiquitous biogenic RONO₂ such as isoprene and terpene RONO₂ which often bear conjugated carbonyl groups (Müller et al., 2014; Shen et al., 2021).

RONO₂ are not only present in the gas phase, as some of them are low volatile compounds and thus partition into condensed phases. As a result, they represent a fraction ranging from 5 to 77 % of the submicron organic aerosol (Kiendler-Scharr et al., 2016; Ng et al., 2017). Under dry conditions, RONO₂ are dissolved in the aerosol phase where the matrix is mostly organic. With increasing relative humidity (RH), the particle can be covered by a water layer where RONO₂ (whether it comes from the particle or the gas phase) can partition. In this case, we consider that soluble RONO₂ partitions to the aqueous phase where it exhibits a specific reactivity.

The aqueous-phase reactivity of RONO₂ plays a significant role in their atmospheric fate. The hydrolysis of tertiary and allylic RONO₂ represents a fast and permanent sink of NO_x in the atmosphere (Hu et al., 2011; Darer et al., 2011; Rindelaub et al., 2015). However, only a small fraction (between 9 % and 34 % for α- and β-pinene RONO₂) of the total pool of organic nitrates undergoes hydrolysis (Takeuchi and Ng, 2019; Wang et al., 2021). Aqueous-phase ·OH-oxidation has been reported to be an important sink for non-volatile terpene RONO₂, even though the ·OH attack is more effectively hindered in the aqueous phase than in the gas phase (González-Sánchez et al., 2021). Nevertheless, limited information is available for RONO₂ aqueous-phase photolysis. To our knowledge, only one study investigated the aqueous-phase absorption cross-sections of individual RONO₂ (Romonosky et al., 2015). However, the literature shows no aqueous-phase photolysis quantum yields, and thus no RONO₂ aqueous-phase photolysis rate constants have been determined so far. Furthermore, the photolysis of RONO₂ with conjugated carbonyl groups remains unexplored, despite its high atmospheric relevance.

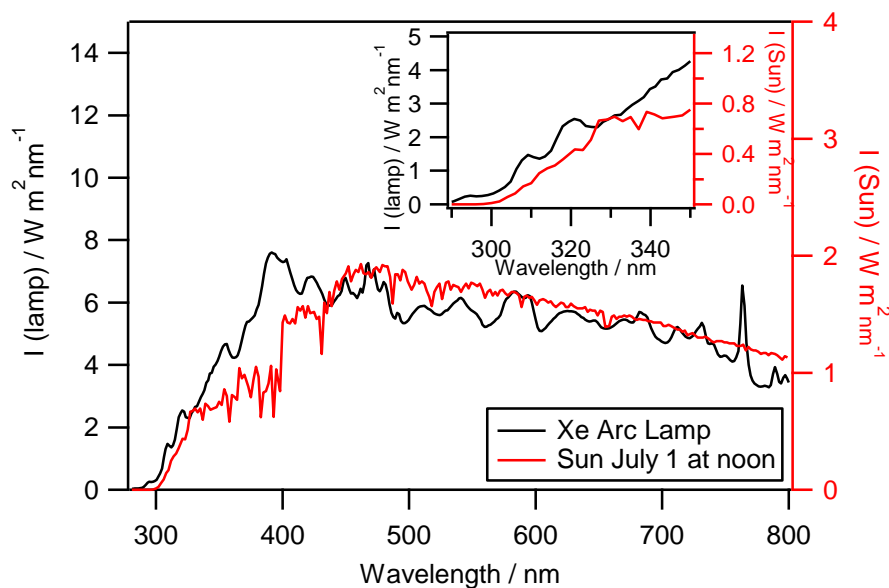
The objective of this work was to determine the aqueous-phase photolysis rate constants of individual RONO₂ including a carbonyl nitrate. Experimental photolysis rate constants of four organic nitrates (isopropyl nitrate, isobutyl nitrate, α-nitrooxyacetone, and 1-nitrooxy-2-propanol) were determined in an aqueous-phase photoreactor, and their average aqueous-

65 phase quantum yields were determined. Then, atmospheric aqueous-phase photolysis rate constants were calculated under various realistic solar light conditions. Finally, using the experimental results, some estimations were performed for the aqueous-phase photolysis rate constants of a set of 45 atmospherically relevant RONO_2 , a global evaluation of all atmospheric sinks in both the gas and the aqueous phase was done, and their atmospheric lifetimes were estimated.

2 Materials and methods

70 2.1 Aqueous-phase photoreactor

The photolysis experiments were performed in a 450 cm^3 double-wall Pyrex aqueous-phase photoreactor (Fig. S1, see details in Renard et al., 2013). The reactor was irradiated by an arc light source (LOT Quantum Design) equipped with a 1000 W arc Xe lamp. Irradiation below 290 nm was removed by an ASTM 892 AM1.5 standard filter. A constant distance (18.4 cm) between the lamp and the water surface was carefully maintained in all experiments using 400 mL of aqueous solution. The Xe arc lamp spectrum is presented in Fig. 1 (black line) and is compared to the solar actinic flux (red line) on the 1st of July 2015 at 40° latitude at ground level. The lamp actinic flux that reaches the photoreactor was measured by an actinometry study with H_2O_2 (detailed in Supplementary Information S1).



80 **Figure 1: Irradiation spectra of the Xe 1000 W arc lamp equipped with an AM1.5 filter (black line) compared to the solar irradiation spectra (red line) on the 1st of July 2015 at 40° latitude at ground level with an overhead ozone column of 300 DU and a surface albedo of 0.1 (using the Tropospheric Ultraviolet (TUV) model, Madronich and Flocke, 1999). Inner graph: zoom on the 290 to 350 nm region.**

2.2 Experimental protocol and determination of experimental RONO₂ photolysis rate constants

Before each photolysis experiment, the photoreactor was filled with 400 mL of ultrapure water and the investigated solubilized compound. The solution was stirred in the dark for 30 min for complete dissolution of the compound. In parallel, the lamp was lighted 10 min before the reaction started to stabilize the light beam. Once the reactor was placed underneath the light beam, the first aliquot was sampled signaling the reaction time zero. Photolysis reactions were performed for 7 h at 298.0 ± 0.2 K and "non-controlled" pH (without buffer solutions). During the reaction time, aliquots were sampled regularly (from 2 to 10 minutes) for offline UHPLC-UV analyses. All the performed photolysis experiments, including experimental conditions, and kinetic results are appended in Table S2.2. As shown in our previous study (González-Sánchez et al., 2021), isopropyl nitrates and isobutyl nitrate are subject to significant evaporation to the reactor's headspace, and α -nitrooxyacetone is subject to hydrolysis. Therefore, control experiments (under dark conditions) were performed to subtract the evaporation and/or hydrolysis kinetic contributions (see Table S2.3). Furthermore, slight quantities of $\cdot\text{OH}$ radicals were formed during the photolysis experiments (via photolysis of the produced HNO₂ and NO₂⁻). Since $\cdot\text{OH}$ radicals react with RONO₂ (González-Sánchez et al., 2021), their attack was considered (Eq. (1)) to precisely determine the RONO₂ aqueous-phase photolysis rate constant.

$$\ln \frac{[\text{RONO}_2]_0}{[\text{RONO}_2]_t} = k' \cdot t = (J_{\text{RONO}_2} + k_{vap/hyd} + k_{OH}[\cdot\text{OH}]) \cdot t, \quad (1)$$

where $[\text{RONO}_2]_0/[\text{RONO}_2]_t$ is the relative decay of aqueous-phase concentrations of the molecule, k' is the pseudo-first-order total decay rate constant (s⁻¹), J_{RONO_2} is the experimental photolysis rate constant (s⁻¹), k_{vap} and k_{hyd} are the experimental evaporation and hydrolysis rate constants (s⁻¹), respectively, k_{OH} is the aqueous-phase $\cdot\text{OH}$ -oxidation rate constant (M⁻¹ s⁻¹), $[\cdot\text{OH}]$ is the aqueous-phase $\cdot\text{OH}$ radical concentration (M) and t is time (s). A detailed explanation of the estimation of $\cdot\text{OH}$ radical concentration is given in SI (Section S2). Note that the contribution of the $\cdot\text{OH}$ oxidation varies with time since $\cdot\text{OH}$ radicals were secondarily formed. Therefore, only data at the beginning of the reaction (< 2 h) were further employed to minimize this contribution. Under these conditions, aqueous-phase $\cdot\text{OH}$ oxidation of RONO₂ accounted for 5 to 10 % of the total decay.

2.3 Analyses of aqueous solutions of RONO₂

The absorption cross-sections of RONO₂ and H₂O₂ in solution were determined from 190 to 340 nm with a UV-Vis-NIR double-beam spectrophotometer (JASCO V670). In addition to the four RONO₂ for which experimental photolysis rate constants were investigated (isopropyl nitrate, isobutyl nitrate, α -nitrooxyacetone, and 1-nitrooxy-2-propanol), the absorption cross-sections of four additional RONO₂ were investigated (1-pentyl nitrate, isopentyl nitrate, 2-ethylhexyl nitrate, and isosorbide 5-mononitrate). Due to low absorption cross-sections above 290 nm, a 5 cm path length cell was used, and due to the low water solubility of some RONO₂, methanol or methanol/water mixture was used as a solvent. The solvents' effects on

the absorption cross-sections were investigated for isopropyl nitrate. Table S1 lists the solvents and ranges of concentrations used to investigate the absorption cross-sections of each RONO_2 (and also H_2O_2)

115 The investigated organic nitrates showed an intense UV absorption band around 200 nm (Fig. S2). During the photolysis experiments, isopropyl nitrate, isobutyl nitrate, α -nitrooxyacetone, and 1-nitrooxy-2-propanol were monitored by UHPLC-UV. The instrument was a Thermo Scientific Accela 600 equipped with a Hypersil Gold C18 column (50×2.1 mm) with a particle size of 1.9 μm and an injection loop of 5 μL at 200 nm. A binary eluent of H_2O and CH_3CN was used for all analyses at a flow rate of 400 $\mu\text{L min}^{-1}$. Two gradients were used depending on the compounds' polarity. For α -nitrooxyacetone and 1-
120 nitrooxy-2-propanol, the gradient started from $\text{H}_2\text{O}/\text{CH}_3\text{CN}$ 90/10 (v/v) to 50/50 (v/v) for 3 min, held at this proportion for 1 min, and then set back to 90/10 (v/v) within 10 s until the end of the run, at minute 5. For isopropyl nitrate and isobutyl nitrate, a similar gradient was employed but the initial and final proportions were $\text{H}_2\text{O}/\text{CH}_3\text{CN}$ 80/20 (v/v).
Calibration curves were optimized to obtain good linearity between 5×10^{-5} and 1×10^{-3} M with an $R^2 > 0.9995$. The retention times were 0.9, 1.2, 2.4, and 3.33 min for 1-nitrooxy-2-propanol, α -nitrooxyacetone, isopropyl nitrate, and isobutyl nitrate
125 respectively. Limits of detection were 1×10^{-5} M for 1-nitrooxy-2-propanol, and α -nitrooxyacetone, and 9×10^{-6} M for isopropyl nitrate and isobutyl nitrate.

2.4 Reagents

Chemicals were commercially available and used as supplied: isopropyl nitrate (96%, Sigma Aldrich), isobutyl nitrate (98%, Sigma Aldrich), 2-ethylhexyl nitrate (97%, Sigma Aldrich), 1-pentyl nitrate (98%, TCI Chemicals), isopentyl nitrate (98%,
130 TCI Chemicals), isosorbide 5-mononitrate (98%, Acros Organics), H_2O_2 (30%, non-stabilized, Acros Organics). Non-commercially RONO_2 , α -nitrooxyacetone, and 1-nitrooxy-2-propanol were synthesized and purified (see SI Section S3). LC/MS grade Acetonitrile (Fisher Optima) was used as supplied. Tap water was purified with a Millipore MiliQ system (18.2 $\text{M}\Omega$ cm and $\text{TOC} < 2$ ppb).

3 Results and discussions

135 3.1 Liquid-phase absorption cross-sections of RONO_2

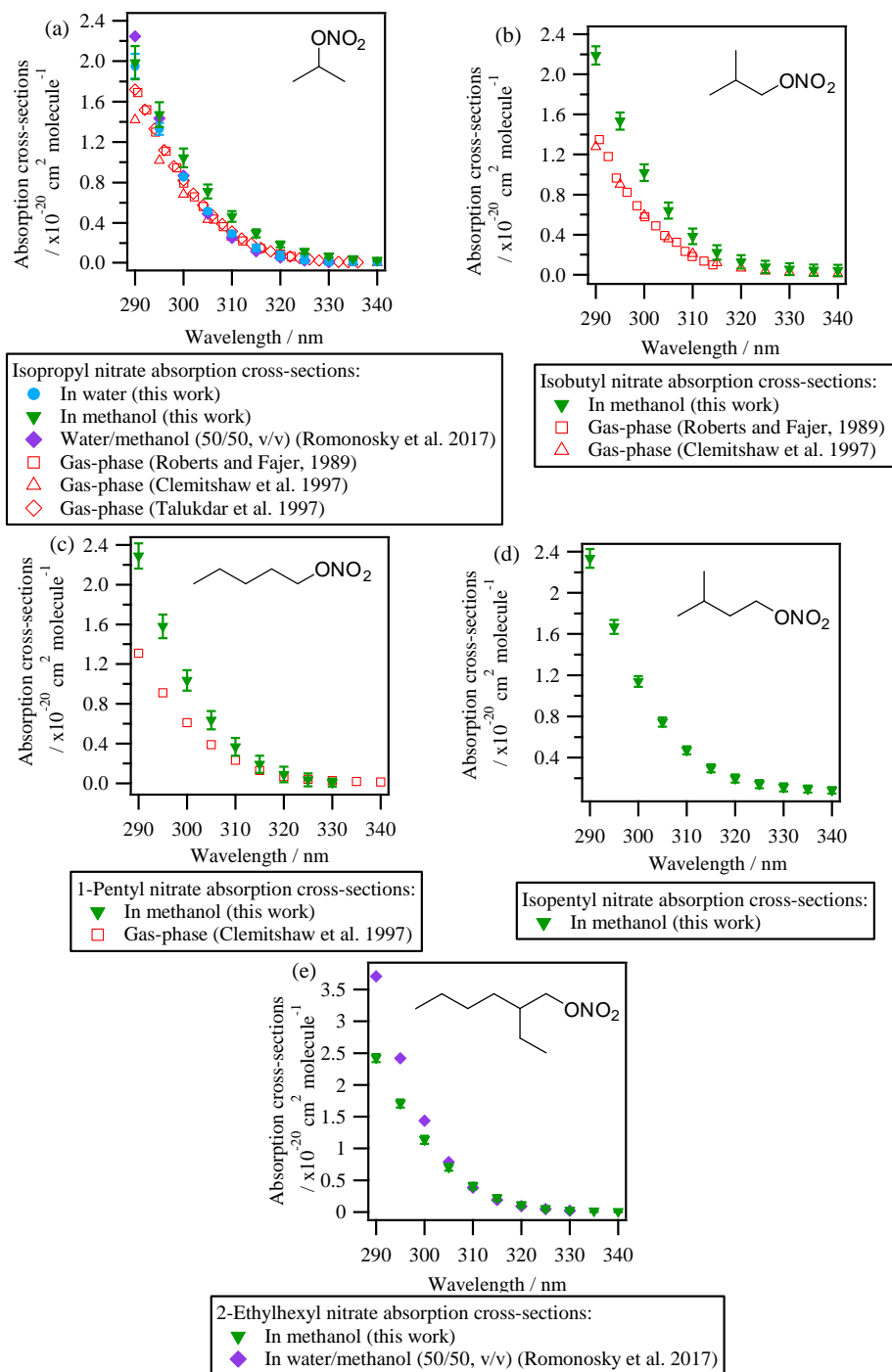
UV-Vis absorbance was investigated for eight organic nitrates (i.e., isopropyl nitrate, isobutyl nitrate, 1-pentyl nitrate, isopentyl nitrate, 2-ethylhexyl nitrate, α -nitrooxyacetone, 1-nitrooxy-2-propanol, and isosorbide 5-mononitrate) dissolved in water or methanol. All RONO_2 absorbed UV light between 190 nm and 330 nm, with maximum absorption at 210 nm due to the $\pi \rightarrow \pi^*$ transition (see Fig. S2). At longer wavelengths, the absorption is produced due to an $n \rightarrow \pi^*$ transition. This
140 transition appears as a shoulder of the $\pi \rightarrow \pi^*$ transition and extends up to ~ 330 nm. The $n \rightarrow \pi^*$ transition is responsible for the light absorption at $\lambda \geq 290$ nm, and thus, is relevant for the atmospheric photolysis of RONO_2 . The determination of the liquid-phase absorption cross-sections of RONO_2 is detailed in SI (Section S4) and all values are compiled in Table S2.

3.1.1. Liquid-phase absorption cross-sections of alkyl nitrates

Figure 2 shows the absorption cross-sections determined for all investigated alkyl nitrates and are compared to those reported in the literature (both in the liquid and the gas phase). Since the absorption cross-sections of alkyl nitrates were mostly investigated in methanol due to their low water solubilities, the absorption cross-sections of isopropyl nitrate in water were compared to that in methanol. The comparison showed that there is a slight shift to shorter wavelengths (blue shift) when isopropyl nitrate is dissolved in water (~ 5 nm in the most impacted region). This shift is likely caused by the stabilization of the non-bonding orbital with increasing solvent polarity. Since this stabilization lowers the ground state energy, the $n \rightarrow \pi^*$ transition energy increases, and thus shorter wavelengths are needed to promote the electron.

It can be concluded from Fig. 2 that all the investigated alkyl nitrates showed similar absorption cross-sections in the liquid phase. The absorption cross-sections determined for isopropyl nitrate are in good agreement with those determined by Romonosky et al., (2015). However, for 2-ethylhexyl nitrate, slightly lower values were obtained in this work at $\lambda < 300$ nm, even though a more polar solvent was used in our work, the reason for this difference is not clear.

Compared to the gas-phase absorption cross-sections, isobutyl nitrate and 1-pentyl nitrate present a ~ 40 % increase in solution. For isopropyl nitrate this increase is less important, the absorption cross-sections are $\sim 25\%$ higher in methanol and nearly identical in water.



160 **Figure 2: Absorption cross-sections of alkyl nitrates in methanol and/or water. Gas-phase absorption cross-sections are included (in red) when available (for isopropyl nitrate, isobutyl nitrate, and 1-pentyl nitrate).**

3.1.2. Liquid-phase absorption cross-sections of polyfunctional RONO₂

Figure 3 shows the absorption cross-sections determined for the investigated polyfunctional RONO₂ dissolved in water or water/methanol. 1-Nitrooxy-2-propanol (Fig. 3b) and isosorbide 5-mononitrate (Fig. 3c) presented absorption cross-section values similar to the investigated alkyl nitrates (Fig. 2). In contrast, α -nitrooxyacetone absorption cross-sections (Fig. 3a) were around five times higher (note the different scale used for this molecule) due to the conjugation of the carbonyl and the nitrooxy group. Furthermore, there are differences in the shape of its spectra: a large shoulder is observed from 320 to 390 nm. This band is not observed in the gas phase and thus it might be caused by interactions between the two chemical groups and the solvent, or it could correspond to an impurity that remained after synthesis, even after purification.

For isosorbide 5-mononitrate absorption cross-sections, the values observed in this work were similar to those determined by Romonosky et al., (2015), although our values were slightly lower at $\lambda > 310$ nm.

Comparison between liquid- and gas-phase absorption cross-sections show that UV absorption is significantly enhanced when polyfunctional RONO₂ are in solution. For α -nitrooxyacetone, this enhancement is of a factor of 2 compared to the values determined by Barnes et al., (1993) and Roberts and Fajer, (1989).

The absorption cross-sections of 1-nitrooxy-2-propanol have not been investigated in the gas phase. Fig. 3b compares its aqueous-phase absorption cross-sections with those of gas-phase 1-nitrooxyethanol (in red in Fig. 3b), determined by Roberts and Fajer, (1989). The only other β -hydroxy RONO₂ for which gas-phase absorption cross-sections were investigated, i.e., *trans*-2-nitrooxy-1-cyclopentanol, is not shown here since the molecule does not absorb UV light above 275 nm (Wängberg et al., 1996).

Fig. 3d displays the absorption cross-sections of six additional β -hydroxy RONO₂ (listed in Table 2) in solution. Overall, Fig. 3b and 3d show that the absorption cross-sections are higher by an order of magnitude for molecules in solution compared to the gas phase. These observations suggest that the nitrate group absorption is likely hindered by the hydroxy group in the gas phase but not in solution, probably due to solvent effects. Nevertheless, gas-phase absorption cross-sections should be determined for other hydroxy RONO₂ to confirm this hypothesis. This is of special atmospheric relevance since β -hydroxy nitrates are formed *via* the addition of \cdot OH radicals to atmospherically relevant unsaturated molecules (such as terpene nitrates and aromatic nitrates, for example) and may significantly partition between the gas and the condensed phases in the atmosphere.

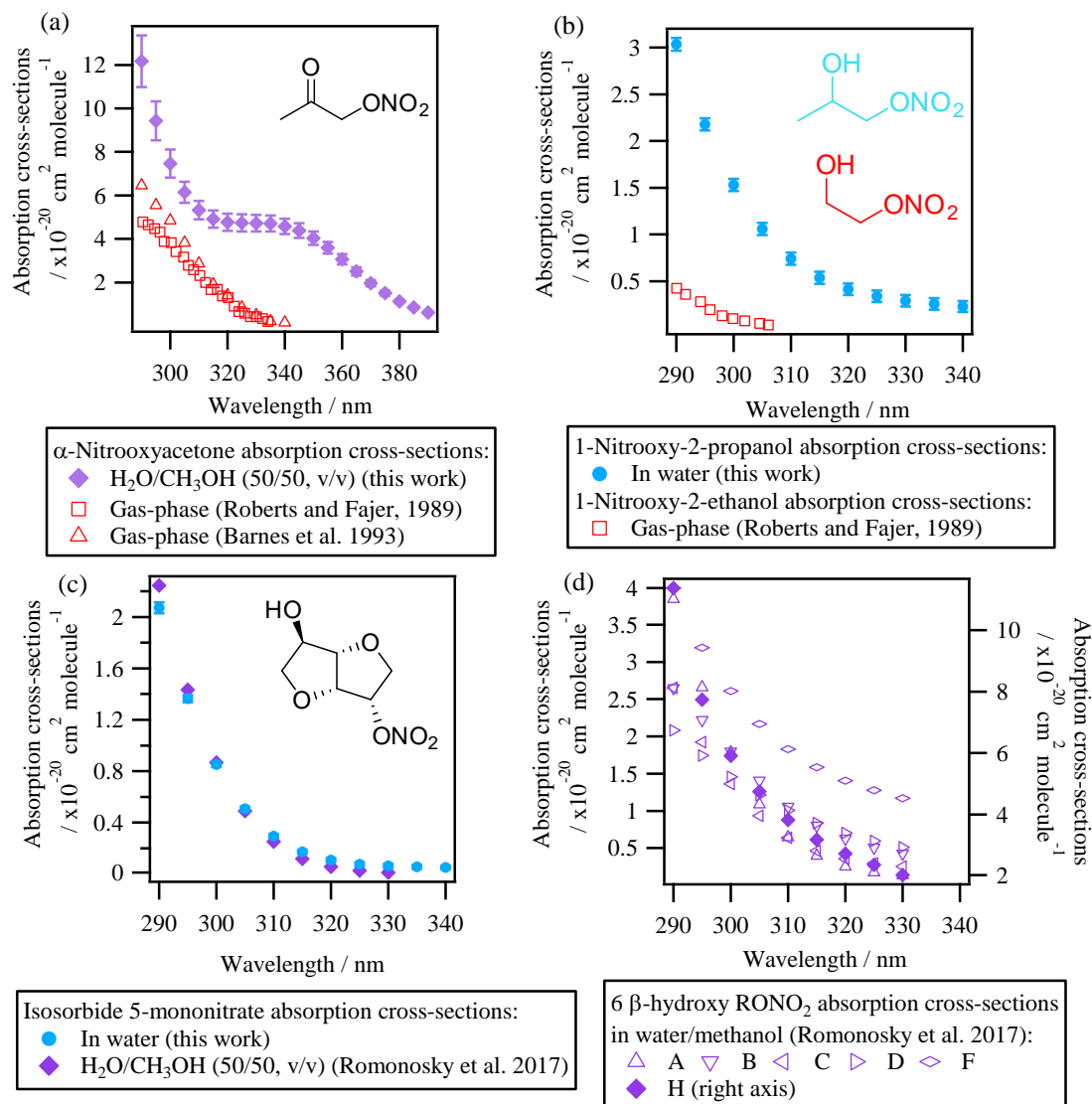


Figure 3: Absorption cross-sections of polyfunctional RONO_2 in water or water/methanol determined in this work and in Romonosky et al., (2015). Gas-phase absorption cross-sections of polyfunctional RONO_2 are included when available (for α -nitrooxyacetone, and 2-nitrooxyethanol). β -Hydroxy nitrates A, B, C, D, F, and H are listed in Table 2.

195 3.2 Liquid-phase photolysis quantum yields of RONO_2

The photolysis quantum yields of RONO_2 were estimated in the liquid phase for the first time. For that purpose, the maximum theoretical photolysis rate constants of RONO_2 were calculated assuming quantum yields of unity and then compared with the experimentally determined ones.

The maximum theoretical photolysis rate constants of RONO_2 under our experimental conditions were calculated using Eq.

200 (3):

$$J_{calc} = \int \sigma(\lambda)\Phi(\lambda) I(\lambda)d\lambda, \quad (3)$$

where J_{calc} is the calculated photolysis rate constant (s^{-1}), $I(\lambda)$ the corrected lamp actinic flux ($photons\ s^{-1}\ cm^{-2}\ nm^{-1}$), and $\Phi(\lambda)$ the quantum yield (assumed equal to one). Since the calculated values represented maximum rate constants using liquid-phase quantum yields of unity, Eq. (4) was used to estimate the actual quantum yields, assuming a constant value over 290 – 340 nm.

$$\Phi = \frac{J_{exp}}{J_{calc}}, \quad (4)$$

where J_{exp} is the experimental rate constant (s^{-1} , Table 1).

Quantum yields are given only for isopropyl nitrate, isobutyl nitrate, α -nitrooxyacetone, and 1-nitrooxy-2-propanol (investigated for J_{exp}). Furthermore, for each molecule, while quantum yields may vary with λ , an average quantum yield was determined over atmospherically relevant wavelengths (290 to 340 nm). Wavelength-resolved quantum yields might be important for α -nitrooxyacetone since two distinct absorbance bands were observed at the investigated wavelengths (Fig. 3). Additionally, isobutyl nitrate and α -nitrooxyacetone photolysis rate constants might be overestimated due to the solvent used for the determinations of their absorption cross-sections. Indeed, for isopropyl nitrate, a 60 % increase in the calculated photolysis rate constant was observed when dissolved in methanol as compared to water (Table 1). However, no corrections were performed for isobutyl nitrate and α -nitrooxyacetone since the enhancement reported for isopropyl nitrate cannot be generalized to other molecules.

Table 1. Calculated and experimental photolysis rate constants of RONO₂ in the liquid phase, estimated liquid-phase quantum yields (Φ), and comparison with gas-phase Φ .

RONO ₂	Solvent for J_{calc}	J_{calc} ($\times 10^{-5}\ s^{-1}$)	J_{exp} ($\times 10^{-5}\ s^{-1}$)	Liquid-phase Φ	Gas-phase Φ
Isopropyl nitrate	water	1.69 ± 0.43	0.50 ± 0.10	0.29 ± 0.09	1.00 ± 0.05^a
	methanol	2.86 ± 0.38			
Isobutyl nitrate	methanol	2.43 ± 0.89	0.94 ± 0.34	0.39 ± 0.20	1^c
1-Pentyl nitrate	methanol	1.92 ± 0.69			
Isopentyl nitrate	methanol	3.30 ± 0.52			
2-Ethylhexyl nitrate	methanol	2.31 ± 0.41			
Isosorbide 5-mononitrate	water	2.12 ± 0.20			
1-Nitrooxy-2-propanol	water	6.16 ± 0.85	0.40 ± 0.04	0.07 ± 0.01	1^c
α -Nitrooxyacetone	water/methanol	172 ± 16	0.31 ± 0.02	0.002 ± 0.001	0.9^b

^aExperimentally determined at 308, 315, and 320 nm by Carbajo and Orr-Ewing, (2010). ^bEstimated by Müller et al., (2014) out of data from Suarez-Bertoa et al., (2012). ^cAssumed to be similar to alkyl nitrates gas-phase Φ .

Table 1 shows the calculated and experimental photolysis rate constants along with the estimated quantum yields. It clearly shows that the maximum calculated values (J_{calc}) were similar for all compounds, except for 1-nitrooxy-2-propanol and α -nitrooxyacetone. These compounds presented much higher values due to their stronger UV absorption. In contrast, the aqueous-phase experimental photolysis rate constants were of the same order of magnitude for the four investigated $RONO_2$, and no increase associated with the presence of any functional group adjacent to the nitrate group was observed.

Table 1 also shows that quantum yields are much lower in the liquid phase than in the gas phase. The estimated quantum yields are ~ 3 , ~ 15 , and ~ 500 times lower in solution for alkyl nitrates, 1-nitrooxy-2-propanol, and α -nitrooxyacetone, respectively. This observation is coherent with previous studies showing that the photolysis quantum yields in the aqueous phase are usually lower than those in the gas phase, as shown, for example, for H_2O_2 or HNO_3 (Herrmann, 2007; Bianco et al., 2020; Romer et al., 2018). This can be caused by the solvent cage effect. When a molecule is photolyzed in a solvent, its photolysis products are trapped by the surrounding solvent molecules. This solvent cage eases the reconversion of the products into the original molecule, and thus decreases the overall quantum yield. Additionally, excited molecules can easily lose the gained energy by colliding with the surrounding solvent molecules.

Although the absorption cross-sections of polyfunctional $RONO_2$ such as α -nitrooxyacetone and 1-nitrooxyacetone are enhanced in solution, the enhancement does not imply an increase in their photolysis rate constants since their quantum yields are also lower in solution. The same effect has been reported for the photolysis of NO_3^- in bulk aqueous solutions when compared to the gas-phase photolysis of HNO_3 (Svoboda et al., 2013; Warneck and Wurzinger, 1988; Nissenson et al., 2010). For α -nitrooxyacetone, the extremely low quantum yield determined in this work is influenced by the important absorption band observed above 320 nm (Fig. 3). However, even when removing this band from its absorption cross-sections (by deconvolution of the spectra, see SI Section S5), a very low quantum yield was obtained (0.02), lower than any other $RONO_2$ due to its higher absorption between 290 and 320 nm. In any case, the aqueous phase photolysis rate constant of this compound was similar to the other $RONO_2$ despite its much higher UV absorption. This is of special importance since gas-phase photolysis is one of the major sinks for carbonyl $RONO_2$ (Müller et al., 2014). These results indicate that if these compounds effectively partition to the aqueous phase, their photolysis may not be such a relevant sink.

To evaluate the atmospheric impact of aqueous-phase photolysis, its rate constants were calculated under various light conditions for the investigated organic nitrates and seven other $RONO_2$ molecules for which liquid-phase absorption cross-sections were reported by Romonosky et al., (2015).

3.3 Atmospheric aqueous-phase photolysis rate constants of $RONO_2$

Atmospheric aqueous-phase photolysis rate constants were calculated for fourteen $RONO_2$ using Eq. (3) under two different scenarios (Table 2): i) a global scenario (actinic flux with a 60° solar zenith angle), and ii) a summer scenario (actinic flux for the 1st of July at noon at 40° latitude). The latter was investigated to determine the maximum aqueous phase photolysis kinetics of $RONO_2$ under atmospheric conditions. The actinic flux was taken from the Tropospheric Ultraviolet-Visible (TUV) model (Madronich and Flocke, 1999). Other parameters in common for both scenarios were an overhead ozone column of 300 DU,

a surface albedo of 0.1, and a ground elevation of 0 km. Although it has been discussed that light is enhanced in liquid cloud droplets by a factor of two (Madronich, 1987), this enhancement factor was not included here since it can largely fluctuate. Furthermore, the comparison with the gas-phase photolysis rate constants appears clearer if no enhancement factor is included. The investigated RONO₂ comprised five alkyl nitrates, one ketonitrate, and eight hydroxy nitrates including seven β-hydroxy nitrates, and four RONO₂ conjugating more than one functional group (Table 2). The absorption cross-sections were either calculated in this work or taken from Romonosky et al., (2015) who determined the absorption cross-sections of several RONO₂ compounds dissolved in a mixture of water and methanol (50/50, v/v). Using our results shown above (Table 1), a quantum yield of 0.34 (average from isopropyl nitrate and isobutyl nitrate) was applied to all alkyl nitrates and isosorbide 5-mononitrate, a quantum yield of 0.07 was applied for all β-hydroxy nitrates, and a quantum yield of 0.002 was applied for α-nitrooxyacetone.

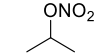
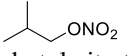
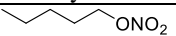
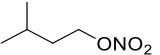
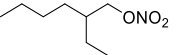
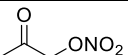
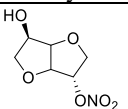
The aqueous-phase photolysis lifetimes were estimated using Eq. (5).

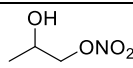
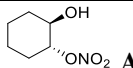
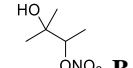
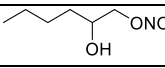
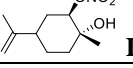
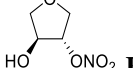
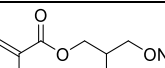
$$\tau_{hv} = \frac{1}{J_{aq} \cdot 86400},$$

(5)

where τ_{hv} is the aqueous-phase photolysis lifetime (in days), and J_{aq} is the aqueous-phase photolysis rate constant (in s⁻¹).

Table 2. Calculated aqueous-phase photolysis rate constants and lifetimes for a series of RONO₂ under two scenarios (global and summer), and comparison with their gas-phase values.

RONO ₂	Aqueous phase				Gas phase	
	J _{global} (x10 ⁻⁷ s ⁻¹)	τ _{hv,global} (d)	J _{summer} (x10 ⁻⁷ s ⁻¹)	τ _{hv,summer} (d)	J _{global} (x10 ⁻⁷ s ⁻¹)	τ _{hv,global} (d)
 Isopropyl nitrate	3.2 ^a 4.2 ^b	36 27	10 14	12 8	8.9 ^c	14
 Isobutyl nitrate	5.9 ^a	20	17	7	5.3 ^d	22
 1-Pentyl nitrate	3.0 ^a	38	11	11	8.9 ^e	13
 Isopentyl nitrate	9.7 ^a	12	25	5		
 2-Ethyl hexyl nitrate	4.4 ^a	26	14	8		
	3.5 ^b	33	12	10		
 α-Nitrooxyacetone	0.56 ^a	210	1.4	77	129 ^f	0.9
 Isosorbide 5-mononitrate	5.6 ^a	21	15	8		
	2.1 ^b	54	7.5	16		

 1-Nitrooxy-2-propanol	4.2 ^a	27	10	11	0.05 ^g	2400
 A	1.8 ^b	66	5.1	23		
 B	4.2 ^b	27	11	10		
 C	2.5 ^b	47	6.6	18		
 D	4.7 ^b	25	12	10		
 F	9.7 ^b	12	24	5		
 H	18 ^b	6	47	2		

Aqueous-phase absorption cross-sections determined in ^athis work, ^bRomonosky et al., (2015). Average gas-phase absorption cross-sections were taken from ^cClemmitshaw et al., (1997), Roberts and Fajer, (1989), and Talukdar et al., (1997); ^dClemmitshaw et al., (1997) and Roberts and Fajer, (1989); ^eClemmitshaw et al., (1997); and ^fBarnes et al., (1993) and Roberts and Fajer, (1989) ^gValue from Roberts and Fajer, (1989) corresponding to 2-nitrooxyethanol.

Table 2 shows that all aqueous-phase photolysis rate constants were similar except for α -nitrooxyacetone, and the molecule labeled **H**. For the latter, absorption cross-sections (determined by Romonosky et al., (2015)) were higher than for all the other investigated RONO₂ (Fig. 3), probably due to the conjugated ester and vinyl groups in the molecule. Likely, this molecule presents a quantum yield lower than 0.07, and thus its photolysis rate constant was probably overestimated in Table 2.

Furthermore, although slight differences were observed between this work and that of Romonosky et al., (2015) for isopropyl nitrate and 2-ethylhexyl nitrate, significant differences were obtained for isosorbide 5-mononitrate. This is due to slightly higher determined absorption cross-sections between 310 and 340 nm (Fig. 3). At these wavelengths, the high intensity of the solar actinic flux provokes a substantial variation in the photolysis rate constants.

The apparent similarities between all the RONO₂ aqueous-phase photolysis rate constants are of special importance since they indicate that RONO₂ molecules show very similar aqueous-phase photolysis lifetimes irrespective of the functional group besides the nitrate function.

Table 2 shows that, in general, aqueous-phase global photolysis lifetimes are quite long (from 6 to 210 d), and thus RONO₂ can remain in the aqueous phase for several days if they do not hydrolyze or undergo other sinks. The aqueous-phase photolysis lifetimes are shortened by a factor between 2.4 and 3.5 when using a solar spectrum at noon on the 1st of July.

The comparison between the aqueous-phase and the gas-phase photolysis lifetimes shows that lifetimes alkyl nitrates are relatively similar. However, strong deviations are observed for α -nitrooxyacetone and 1-nitrooxy-2-propanol.

α -Nitrooxyacetone presents a much longer photolysis lifetime in the aqueous phase (210 vs. 0.9 d) due to the extremely low photolysis quantum yield in the aqueous phase (0.002). This implies that the aqueous-phase photolysis is a negligible sink for

295 α -nitrooxyacetone. As mentioned above, gas-phase photolysis is the major sink for carbonyl nitrates as their kinetics are enhanced by the conjugation of the nitrate and the carbonyl group. Our results show that this enhancement is hindered in the aqueous phase, and thus photolysis might not be the major sink for carbonyl nitrates partitioning to the aqueous phase. Conversely, the pair of β -hydroxynitrates compared (1-nitrooxy-2-propanol and 2-nitrooxyethanol) show a much shorter lifetime in the aqueous phase (16 vs. 2400 d) due to a large increase in the absorption cross-sections (Fig. 3). Therefore, the photolysis sink of β -hydroxynitrates is likely greatly enhanced if they partition to the atmospheric aqueous phase. Nevertheless, 300 the obtained very long lifetimes suggest that aqueous-phase photolysis remains a negligible sink. To investigate the relative importance of the aqueous-phase photolysis in the RONO_2 atmospheric fate, the multiphase lifetimes of several atmospherically relevant RONO_2 were calculated, as exposed in the next section.

4 Atmospheric implications

4.1 Photochemical sink contributions to RONO_2 multiphase lifetimes

305 Multiphase photochemical lifetimes were calculated for 32 non-hydrolyzable atmospherically relevant RONO_2 classified in three families according to their VOC precursor and water solubility: six small RONO_2 (isopropyl nitrate, isobutyl nitrate, 1-pentyl nitrate, isopentyl nitrate, 1-nitrooxy-2-propanol, and nitrooxyacetic acid) with low to intermediate water solubilities ($K_H \sim 10^{-1}$ to 10^5 M atm^{-1}), five isoprene nitrates (ethanal nitrate, α -nitrooxyacetone, two methyl vinyl ketone nitrate isomers, and a C_5 dihydroxy dinitrate) with intermediate to high water solubilities ($K_H \sim 10^3$ to 10^7 M atm^{-1}), and twelve terpene nitrates 310 (α - and β -pinene, limonene, γ -terpinene, and myrcene atmospheric reactivity products) with intermediate to very high water solubilities ($K_H \sim 10^4$ to $10^{12} \text{ M atm}^{-1}$). The chemical structures of the investigated RONO_2 and their Henry's Law constants are listed in Table S3.

In the same manner as in González-Sánchez et al., (2021), the multiphase photochemical lifetimes were investigated under two different scenarios: i) under cloud/fog conditions ($\text{LWC} = 0.35 \text{ g m}^{-3}$), and ii) under wet aerosol conditions ($\text{LWC} = 3$ 315 $\cdot 10^{-5} \text{ g m}^{-3}$), using Eq. (6):

$$\tau_{\text{multiphase}} = \frac{1}{\varphi_{aq} J_{aq} + \varphi_{aq} k_{OH,aq} [OH]_{aq} + \varphi_{gas} J_{gas} + \varphi_{gas} k_{OH,gas} [OH]_{gas}}, \quad (6)$$

where φ_{aq} and φ_{gas} is the molar fraction of the compound in the aqueous and the gas phase, respectively; J_{aq} and J_{gas} (s^{-1}) are the global photolysis rate constants (actinic flux with a 60° solar zenith angle) in the aqueous and the gas phase, respectively; $k_{OH,aq}$ and $k_{OH,gas}$ (in $\text{M}^{-1} \text{ s}^{-1}$ and $\text{cm}^3 \text{ molecules}^{-1} \text{ s}^{-1}$, respectively) are the aqueous and gas-phase $\cdot\text{OH}$ - 320 oxidation rate constants; and $[OH]_{aq}$ and $[OH]_{gas}$ (in M and molecules cm^{-3} , respectively) are the $\cdot\text{OH}$ concentrations in each phase.

The calculation of the aqueous and gas phase partitioning is detailed in Section S6.1, where each photolysis and $\cdot\text{OH}$ oxidation rate constants assignments are explained in detail. Briefly, experimental values were used when available; otherwise, they were calculated using group contribution methods (González-Sánchez et al., 2021; Jenkin et al., 2018) or they were assumed

325 based on experimental values of RONO_2 with similar chemical structures. The $\cdot\text{OH}$ concentrations were set to 10^{-14} M in the aqueous phase and $1.4 \cdot 10^6$ molecules cm^{-3} in the gas phase (Tilgner et al., 2013). All K_H values are set at 298 K, as well as all reactivity kinetic rate constants for which most of the activation energies are unknown. Note that lower temperatures should be more realistic, they should mostly affect K_H values, therefore, our results probably underestimate the atmospheric fractioning to the aqueous phase.

330 Figure 4 depicts the RONO_2 multiphase lifetimes under both cloud/fog conditions (Fig. 4a) and wet aerosol conditions (Fig. 4b). The chosen RONO_2 were distributed into three groups according to their nature and source and plotted by increasing water solubility. Figure 4 also shows the aqueous molar fraction of each molecule (in blue) and the relative contribution of each of the investigated sinks to the total multiphase lifetime.

Figure 4 shows much longer multiphase photochemical atmospheric lifetimes for small RONO_2 (from 38 to 264 h) than for isoprene and terpene nitrates (from 2 to 29 h). This is mainly due to their low number of $\cdot\text{OH}$ attack reactive sites, and the absence of highly reactive groups such as aldehyde groups (fast $\cdot\text{OH}$ oxidation) or conjugated carbonyl groups (fast gas-phase photolysis).

The figure also highlights the relevance of aqueous-phase $\cdot\text{OH}$ oxidation, which is the only photochemical sink for RONO_2 partitioning into the aqueous phase. Photolysis is a negligible sink in the aqueous phase, whereas it is an important sink in the gas phase, especially for compounds bearing conjugated carbonyl groups (marked with * in the figure).

340 Figure 4 also shows that RONO_2 multiphase photochemical atmospheric lifetimes can substantially vary under different atmospheric LWC. RONO_2 lifetimes generally increase when the compound effectively partitions to the aqueous phase. This increase is especially important for compounds bearing conjugated carbonyl groups due to the significant difference in their photolysis kinetics between the gas and the aqueous phase. In the gas phase, photolysis is their major sink, while it becomes a minor or even negligible sink when they partition to the aqueous phase. Besides, RONO_2 with no conjugated carbonyl groups tend to show a mild increase in their lifetimes when partitioning to the aqueous phase caused by the deactivation of their $\cdot\text{OH}$ reactivity in water (González-Sánchez et al., 2021).

Comparing Fig. 4a and 4b, very different behaviors are observed depending on the RONO_2 Henry's Law constant. The lifetimes of RONO_2 with low water solubilities ($K_H < 10^4$ M atm^{-1} , i.e., RONO_2 with $\phi_{\text{aq}} \leq 7$ % in Fig. 4a), barely vary between the cloud/fog and the wet aerosol scenarios since their aqueous-phase molar fractions are extremely low.

350 In contrast, for molecules with intermediate to high water solubilities ($K_H = 10^5 - 10^9$ M atm^{-1} , i.e., methyl vinyl ketone isomers, C_5 dihydroxy dinitrate, α -pinene 2–4, β -pinene 2–8, terpinene 1), significant variations between the two scenarios are clearly observed. Their aqueous-phase partitioning ranges from 91 % (on average) under cloud/fog conditions to 12 % (on average) under wet aerosol conditions. Compared to wet aerosol conditions, the increase of photochemical lifetimes under cloud/fog conditions is much more pronounced for RONO_2 bearing conjugated carbonyl groups (lifetimes up to 3 times higher) due to their much slower aqueous phase reactivity.

Finally, very high water-soluble RONO_2 ($K_H \geq 10^{10} \text{ M atm}^{-1}$, i.e., RONO_2 for which $\phi_{\text{aq}} \geq 89\%$ in Fig. 4b) barely partition to the gas phase even under low LWC, and thus, their lifetimes are similar under both conditions. For these RONO_2 , aqueous-phase $\cdot\text{OH}$ oxidation is the main sink, even under wet aerosol conditions with extremely low amounts of water.

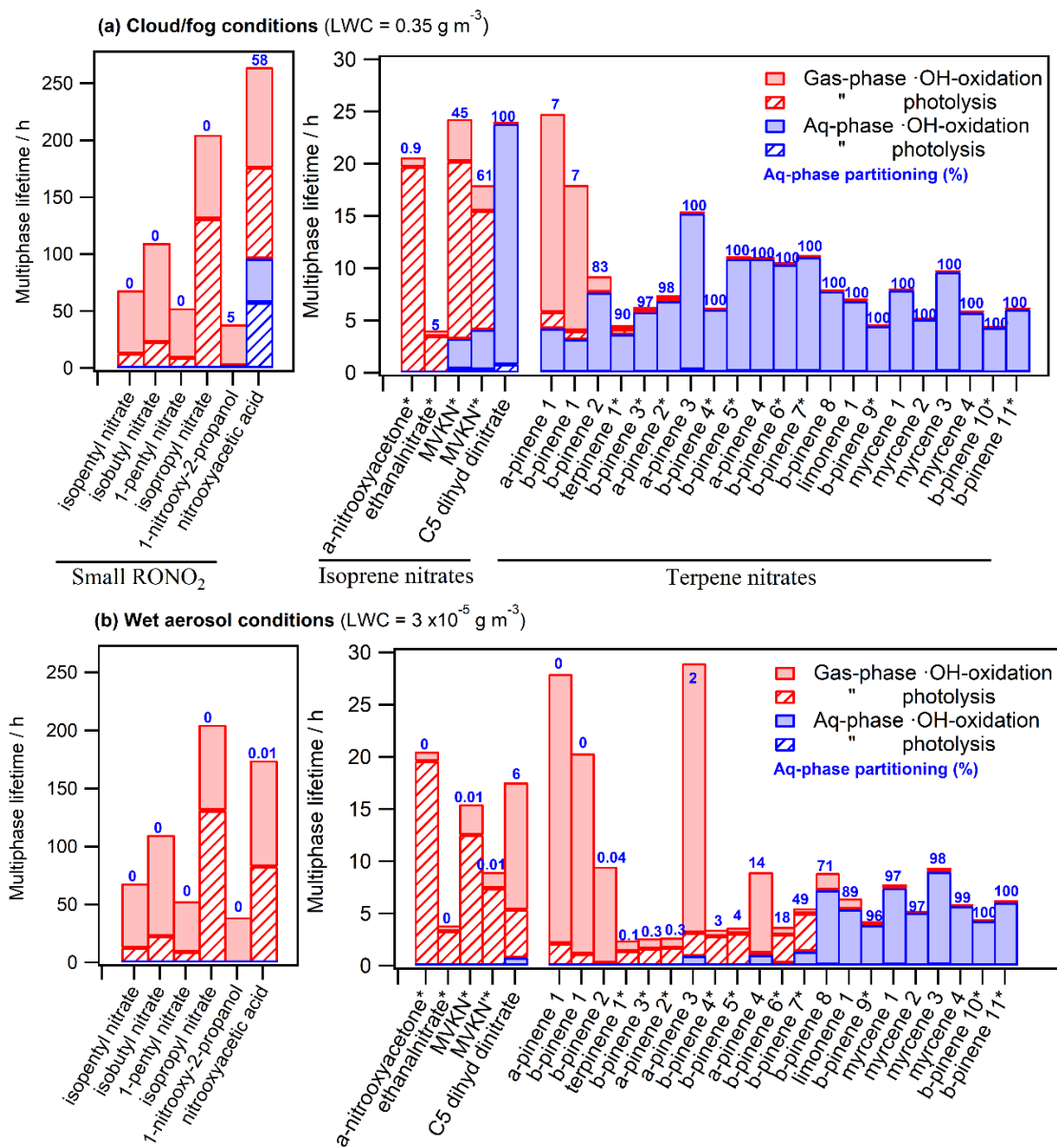


Figure 4: Chemical multiphase lifetimes and relative contribution of each sink for 32 atmospherically relevant RONO_2 distributed into i) small RONO_2 (SN, left axis), ii) isoprene nitrates (IN, right axis), and iii) terpene nitrates (TN, right axis) under (a) cloud/fog conditions ($\text{LWC} = 0.35 \text{ g m}^{-3}$) and (b) wet aerosol conditions ($\text{LWC} = 3 \times 10^{-5} \text{ g m}^{-3}$). The numbers in blue indicate the aqueous-phase molar fraction (in %). *Conjugated carbonyl nitrates. The chemical structures, properties, and kinetic rate constants of each compound are listed in Table S3.

4.2 Importance of hydrolysis in multiphase chemical lifetimes

Hydrolysis is a known process that can influence the atmospheric lifetimes of RONO₂, mostly tertiary and allylic RONO₂. These chemical structures can stabilize the reaction intermediate carbocation formed through the acid-catalyzed unimolecular nucleophilic substitution (S_N1). Other RONO₂ (such as primary or secondary RONO₂) can also undergo hydrolysis under very acidic conditions (Rindelaub et al., 2016; Wang et al., 2021), but these reactions remain extremely slow under atmospheric conditions, and they are considered in this work as “non-hydrolyzable”.

Up to date, the hydrolysis of nine tertiary RONO₂ and four allylic RONO₂ have been experimentally investigated by different authors (Hu et al., 2011; Darer et al., 2011; Jacobs et al., 2014; Rindelaub et al., 2015; Wang et al., 2021), reporting a wide range of hydrolysis rate constants at neutral pH (from $9.9 \cdot 10^{-6}$ to $9.3 \cdot 10^{-3} \text{ s}^{-1}$).

To assess the relative importance of aqueous-phase ·OH-oxidation and photolysis in relation to hydrolysis, the multiphase lifetimes of these RONO₂ were evaluated under the two scenarios (cloud/fog and wet aerosol conditions) using Eq. (8).

$$\tau_{\text{multiphase}} = \frac{1}{\varphi_{aq} \cdot k_{hyd} + \varphi_{aq} \cdot J_{aq} + \varphi_{aq} \cdot k_{OH,aq} \cdot [OH]_{aq} + \varphi_{gas} \cdot J_{gas} + \varphi_{gas} \cdot k_{OH,gas} \cdot [OH]_{gas}} \quad (8)$$

The chemical structures of the investigated compounds are described in Table S4 along with their Henry’s Law constants (from 1 to 10¹⁰ M atm⁻¹) and their hydrolysis rate constants. Assumptions performed to assign photolysis and ·OH oxidation rate constants are detailed in Section S6.2.

Figure 5 displays the hydrolyzable RONO₂ multiphase atmospheric lifetimes in the same manner as in Fig. 4, and it shows that hydrolysis can substantially impact RONO₂ atmospheric removal.

On the one hand, for RONO₂ with high hydrolysis rate constants (*tert* 3, 4, 7, 8, and 9, and *ally* 3 and 4 with $k_{hyd} > 10^{-3} \text{ s}^{-1}$) the hydrolysis is the major sink under cloud/fog conditions even for compounds that barely partition to the aqueous phase (*tert* 3 and 4); while under wet aerosol conditions, it can be a very significant sink (*tert* 7, 8 and 9). These RONO₂ are processed within less than 2 h under cloud/fog conditions, and their atmospheric lifetimes can be shortened by two orders of magnitude with respect to the wet aerosol scenario (only the highly water-soluble *tert* 9 presents similar lifetimes (0.7 h) under both conditions). For these RONO₂, aqueous-phase ·OH oxidation and photolysis are completely irrelevant, and their chemical lifetimes are only driven by hydrolysis or gas-phase reactivity depending on their atmospheric partitioning and hydrolysis rate constants.

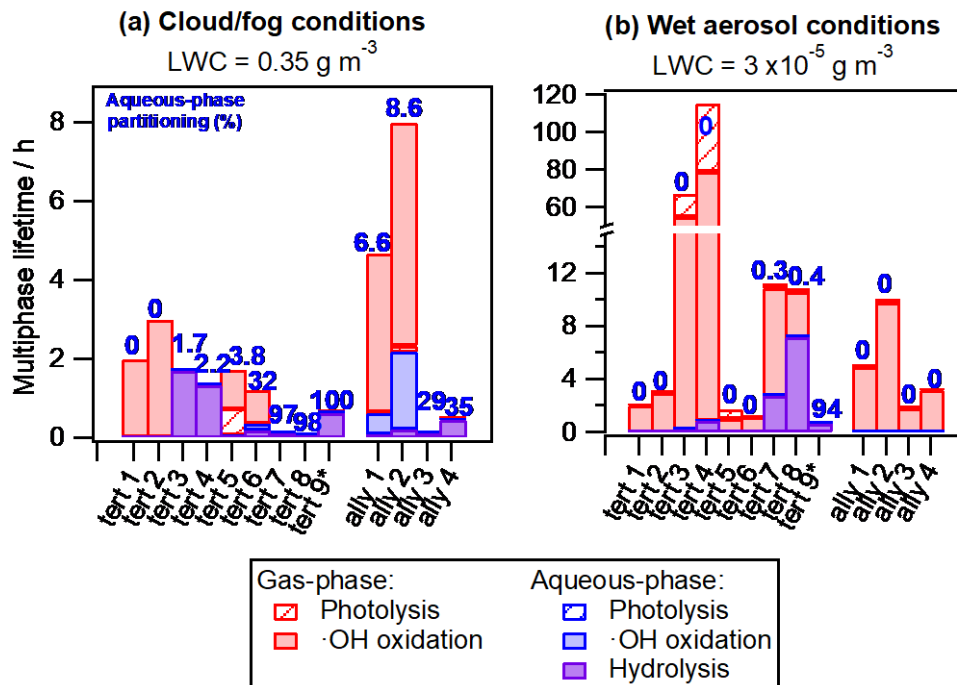


Figure 5: Chemical multiphase lifetimes and relative contribution of each sink of tertiary and allylic RONO₂ under (a) cloud/fog conditions (LWC = 0.35 g m^{-3}) and (b) wet aerosol conditions (LWC = $3 \times 10^{-5} \text{ g m}^{-3}$). The numbers in blue indicate the aqueous-phase molar fraction (in %). The chemical structures, properties, and kinetic rate constants of each compound are listed in Table S4.

On the other hand, for RONO₂ with lower hydrolysis rate constants ($k_{\text{hyd}} < 10^{-4} \text{ s}^{-1}$), aqueous-phase ·OH oxidation can compete with or overcome hydrolysis as a faster sink (*tert* 6, and *ally* 1 and 2 under cloud/fog conditions). Nevertheless, their atmospheric removal is mostly controlled by their gas-phase reactivity due to their low water solubility. However, it is likely that the aqueous-phase ·OH oxidation is an important process for other tertiary and allylic RONO₂ with higher water solubilities, such as RONO₂ bearing carbonyl groups and/or presenting low hyperconjugation since these molecules tend to present longer hydrolysis lifetimes (Wang et al., 2021). This is of high importance since many authors tend to assume short atmospheric lifetimes due to fast hydrolysis (within hours) for large fractions of atmospheric RONO₂ (Fisher et al., 2016; Zare et al., 2019; Browne et al., 2013), while the decay of these RONO₂ can actually be mostly controlled by the aqueous-phase ·OH reactivity.

4.3 Overall RONO₂ multiphase lifetimes

Finally, overall multiphase lifetimes of 45 RONO₂ were calculated by including the contribution of dry and wet deposition using Eq. (9). These 45 compounds were classified into i) non-hydrolyzable small RONO₂, ii) non-hydrolyzable isoprene and terpene nitrates, and iii) hydrolyzable RONO₂.

$$\tau_{\text{multiphase}} = \frac{1}{\varphi_{aq} \cdot k_{\text{hyd}} + \varphi_{aq} \cdot J_{aq} + \varphi_{aq} \cdot k_{OH,aq} \cdot [OH]_{aq} + \varphi_{gas} \cdot J_{gas} + \varphi_{gas} \cdot k_{OH,gas} \cdot [OH]_{gas} + k_{dep}}, \quad (9)$$

410 where k_{dep} is the deposition rate constant (in s^{-1}) that accounts for both dry and wet deposition. The assignment of k_{dep} to each RONO₂ is detailed in Section S6.3.

Figure 6 shows the overall lifetimes of all investigated RONO₂ under both cloud/fog conditions (Fig. 6a), and wet aerosol conditions (Fig. 6b). Furthermore, the relative contribution of each sink (deposition, aqueous-phase reactivity, and gas-phase reactivity) is represented.

415 The results show that all sinks (deposition, aqueous-phase and gas-phase reactivity) significantly contribute to the RONO₂ atmospheric consumption. However, the contribution of each sink and the overall RONO₂ atmospheric lifetimes depend largely on the RONO₂ chemical structure and the LWC. These parameters can thus highly impact the NO_x atmospheric transport. Hereafter, we discuss the results for each class of RONO₂.

Non-hydrolyzable small RONO₂. Due to their low reactivity, they present the highest lifetimes (between 12 and 97 h). These 420 lifetimes barely vary under both investigated scenarios since the compounds hardly partition to the aqueous phase in any scenario. The lifetimes are especially larger for alkyl nitrates since deposition rate constants are much lower. Under these circumstances, alkyl nitrates are the major responsible for NO_x flatter distribution due to their long-range atmospheric transport. Furthermore, its sink is mostly controlled by gas-phase chemistry which is responsible for NO_x recovery.

Non-hydrolyzable isoprene and terpene nitrates. They present shorter lifetimes (between 2 and 15 h) than those of small 425 RONO₂. In general, their atmospheric lifetimes are mostly controlled by chemical sinks although deposition is considerable (38% and 33 % under cloud/fog and wet aerosol conditions, respectively). Their average lifetimes are slightly longer under cloud/fog conditions (6.1 h vs 5.4 h under wet aerosol conditions) due to their lower reactivity in the aqueous phase. This increase in the atmospheric lifetime with increasing LWC is especially important for RONO₂ with intermediate to high water solubility $K_H = 10^5 - 10^9 \text{ M atm}^{-1}$) and the presence of conjugated carbonyl groups (the increase is of up to twice). The less- 430 reactive nature of RONO₂ in the aqueous phase increases the relative contribution of deposition sinks (up to twice) under cloud/fog conditions. Therefore, for this kind of compounds, an LWC increase would result in lower NO_x recycling efficiencies since deposition represent a permanent NO_x sink although RONO₂ are likely transported further. One should also note the importance of aqueous-phase reactivity for terpene nitrates even under wet aerosol conditions. This highlights the importance of understanding the contribution of this reactivity to NO_x formation.

435 **Hydrolyzable RONO₂.** Much shorter lifetimes are estimated under cloud/fog conditions (average 1.6 vs. 4.9 h) mostly due to the fast hydrolysis of RONO₂ with high hydrolysis rate constants (*tert* 1 – 5, and *ally* 3 and 4). The atmospheric lifetimes of these RONO₂ can be shortened by two orders of magnitude. Due to the shortening on their atmospheric lifetimes and the irreversible loss of the nitrate group through hydrolysis, these RONO₂ likely transport much less effectively NO_x at increasing LWC.

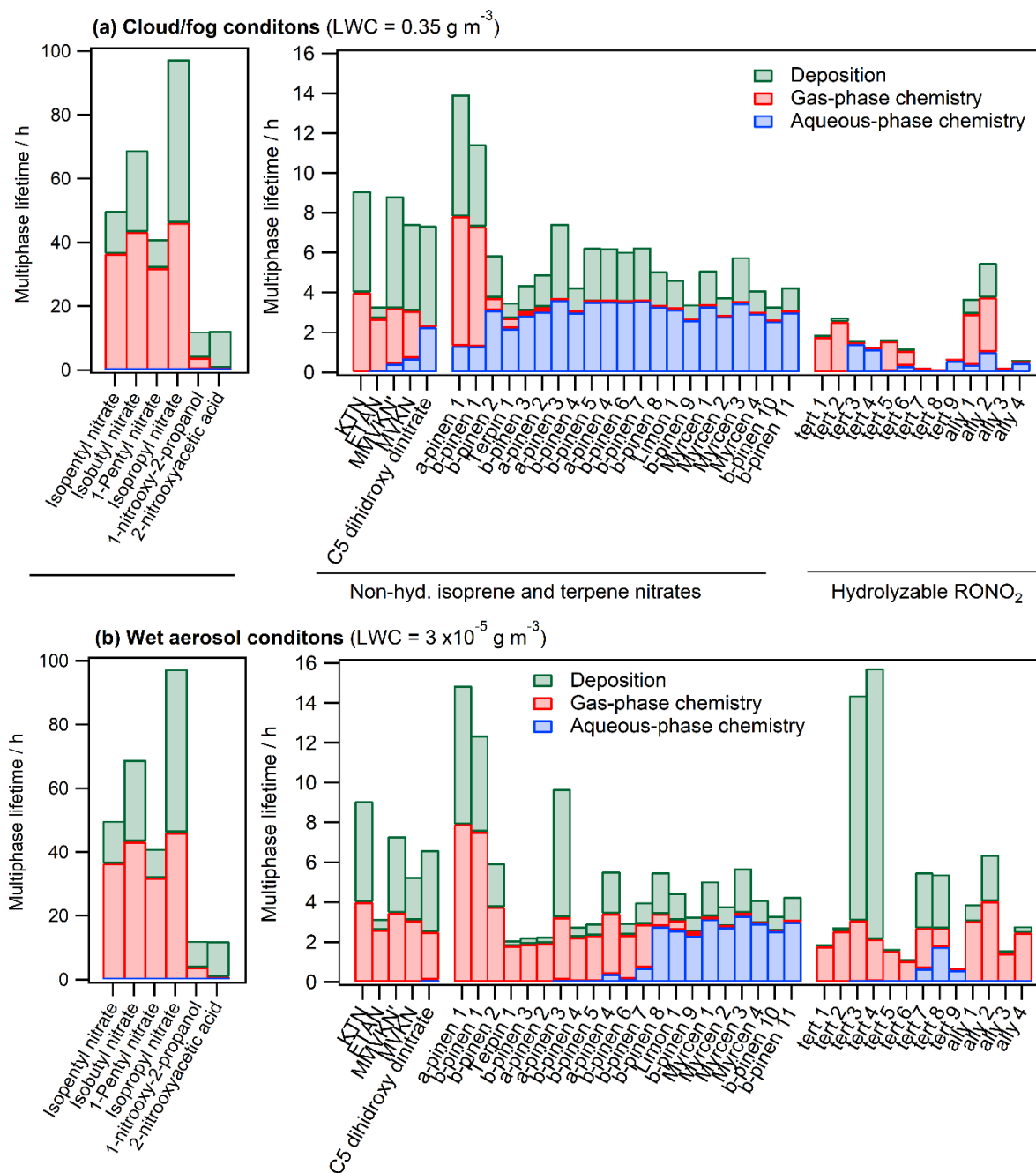


Figure 6: Multiphase atmospheric lifetimes and relative contributions of each sink for 45 atmospherically relevant $RONO_2$ distributed into i) non-hydrolyzable small $RONO_2$ (SN), ii) non-hydrolyzable isoprene nitrates (IN) and terpene nitrates (TN), and iii) hydrolyzable $RONO_2$ (HN) under (a) cloud/fog conditions ($LWC = 0.35 \text{ g m}^{-3}$), and (b) wet aerosol conditions ($LWC = 3 \times 10^{-5} \text{ g m}^{-3}$).

445 5 Conclusions

Photolysis rate constants and quantum yields were determined in the liquid phase for the first time for isopropyl nitrate, isobutyl nitrate, α -nitrooxyacetone, and 1-nitrooxy-2-propanol. Photolysis of these compounds was shown to be hindered in the liquid phase compared to the gas phase. Although they generally presented higher absorption cross-sections when dissolved in the liquid phase, lower quantum yields were observed compared to the gas phase (0.002–0.39 versus ~ 1), probably due to solvent cage effects.

Furthermore, no significant differences were observed in the aqueous-phase photolysis rate constants between various RONO_2 containing a carbonyl group, a hydroxy group, or none of them. In contrast, previous studies have shown that the gas-phase photolysis of RONO_2 is greatly enhanced for α - or β -carbonyl nitrates. Our results showed much lower photolysis rates for carbonyl nitrates in the aqueous phase and thus, longer photolysis atmospheric lifetimes than in the gas phase. This is of special relevance for these compounds in the atmosphere since photolysis is expected to be their major sink.

Considering two different scenarios: i) cloud/fog conditions ($\text{LWC} = 0.35 \text{ g m}^{-3}$) and ii) wet aerosol conditions ($\text{LWC} = 3 \times 10^{-5} \text{ g m}^{-3}$), a complete evaluation of the atmospheric sinks of 45 RONO_2 was performed, including aqueous- and gas-phase $\cdot\text{OH}$ -oxidation and photolysis, hydrolysis, and dry and wet deposition. The results highlighted the importance of aqueous-phase $\cdot\text{OH}$ oxidation, a major sink for some RONO_2 even under low LWC, whereas aqueous-phase photolysis remained of negligible importance. The results also emphasized the influence of the RONO_2 chemical structure on RONO_2 atmospheric fate and thus their ability to transport NO_x . The chemical structure of each RONO_2 can influence the kinetics of its multiphase reactivity, and its partitioning between the aqueous and the gas phase.

Small RONO_2 such as alkyl nitrates barely partition into the aqueous phase (even under high LWC conditions). Furthermore, they present low gas-phase reactivity due to their low number of reactive sites and absence of highly reactive groups. Hence, these RONO_2 present the longest lifetimes and thus, are responsible for the NO_x flatter distribution.

The atmospheric fate of polyfunctional RONO_2 such as isoprene and terpene nitrates highly depends on their chemical structure. Some tertiary and allylic RONO_2 present very high hydrolysis rate constants ($k_{\text{hyd}} > 5 \cdot 10^{-4} \text{ s}^{-1}$). For these compounds, hydrolysis is the only sink even when they mildly partition to the aqueous phase ($\phi_{\text{aq}} > 0.4 \%$). Their atmospheric lifetimes can decrease drastically (up to two orders of magnitude) with increasing LWC, and under these conditions, their processing represents a net sink of NO_x . Out of these results, it is evident that more research should be done to clearly elucidate the influence of the RONO_2 chemical structure on the hydrolysis rate constant.

The fate of polyfunctional RONO_2 with low or negligible hydrolysis ($k_{\text{hyd}} < 1 \cdot 10^{-4} \text{ s}^{-1}$) is mainly controlled by their atmospheric partitioning. For molecules with low water solubility ($K_{\text{H}} < 10^4 \text{ M atm}^{-1}$), their fate is mainly controlled by their gas-phase reactivity and dry deposition. Their atmospheric lifetimes are lower than those of alkyl RONO_2 (ranging from 2 to 15 h) and are impacted by the presence of conjugated carbonyl groups (fast photolysis), and aldehyde groups, and double bonds (fast $\cdot\text{OH}$ -oxidation). They may thus recycle NO_x . RONO_2 with intermediate water solubilities ($K_{\text{H}} = 10^5 - 10^9 \text{ M atm}^{-1}$) show more complex processing, their atmospheric fate and lifetimes highly depend on the LWC. At high LWC, their sink

is mainly controlled by aqueous-phase $\cdot\text{OH}$ oxidation and dry and wet deposition, while at low LWC gas-phase $\cdot\text{OH}$ oxidation and photolysis are the main sinks. Due to the decrease of the RONO_2 reactivity in condensed phases, their atmospheric lifetimes increase with increasing LWC (up to twice greater). Furthermore, the overall importance of non-chemical sinks (deposition) increases with higher LWC. The ability of RONO_2 aqueous-phase $\cdot\text{OH}$ -oxidation to recycle NO_x must be investigated to properly predict the impact of their fate, especially since they represent an important fraction of the atmospherically relevant RONO_2 . Finally, RONO_2 with very high water solubility ($K_H \geq 10^{10} \text{ M atm}^{-1}$) partition to the aqueous phase even under very low LWC, and thus their fate is mainly controlled by aqueous-phase $\cdot\text{OH}$ oxidation, dry and wet deposition.

Data availability. All data related to this article are available at <https://doi.org/10.7910/DVN/O7HKJQ>.

Author contributions. JMGS performed all kinetic experiments, treated all data, and built the atmospheric implication discussion. NB provided the UV-VIS data for RONO_2 . JMGS and SR developed the UHPLC-UV method for RONO_2 . JMGS and JLC performed the organic synthesis of RONO_2 . AM and JLC led the work. JMGS, AM, and JW wrote the article with inputs from all co-authors.

Competing interests. The authors declare that they have no conflict of interest.

Acknowledgements. The authors thank Camille Mouchel-Vallon for his help using the GECKO-A modelling tool.

Financial support. This project has received funding from the European Union's Horizon 2020 research and innovation program under the Marie Skłodowska-Curie (grant no. 713750). It has been carried out with the financial support of the Regional Council of Provence-Alpes-Côte d'Azur and with the financial support of the A*MIDEX (grant no. ANR-11-IDEX-0001-02), funded by the Investissements d'Avenir project funded by the French Government, managed by the French National Research Agency (ANR). This study also received funding from the French CNRS-LEFE-CHAT (Programme National-Les Enveloppes Fluides et l'Environnement-Chimie Atmosphérique – Project “MULTINITRATES”). The authors also acknowledge the support from the French National Research Agency (ANR-PRCI) through the projects PARAMOUNT (ANR18-CE92-0038-02) ORACLE (ANR-20-CE93-0008-01_ACT) and AEROFOG (ANR-22-CE92-0051).

References

Atkinson, R. and Aschmann, S. M.: Rate constants for the reactions of the OH radical with the propyl and butyl nitrates and 1-nitrobutane at $298 \pm 2 \text{ K}$, *Int J Chem Kinet*, 21, 1123–1129, <https://doi.org/10.1002/kin.550211205>, 1989.

Barnes, I., Becker, K. H., and Zhu, T.: Near UV absorption spectra and photolysis products of difunctional organic nitrates: Possible importance as NO_x reservoirs, *J Atmos Chem*, 17, 353–373, <https://doi.org/10.1007/BF00696854>, 1993.

- 510 Bedjanian, Y., Morin, J., and Romanias, M. N.: Reactions of OH radicals with 2-methyl-1-butyl, neopentyl and 1-hexyl nitrates. Structure-activity relationship for gas-phase reactions of OH with alkyl nitrates: An update, *Atmos Environ*, 180, 167–172, <https://doi.org/10.1016/j.atmosenv.2018.03.002>, 2018.
- Bianco, A., Passananti, M., Brigante, M., and Mailhot, G.: Photochemistry of the cloud aqueous phase: A review, <https://doi.org/10.3390/molecules25020423>, 20 January 2020.
- 515 Browne, E. C., Min, K.-E., Wooldridge, P. J., Apel, E., Blake, D. R., Brune, W. H., Cantrell, C. A., Cubison, M. J., Diskin, G. S., Jimenez, J. L., Weinheimer, A. J., Wennberg, P. O., Wisthaler, A., and Cohen, R. C.: Observations of total RONO₂ over the boreal forest: NO_x sinks and HNO₃ sources, *Atmos Chem Phys*, 13, 4543–4562, <https://doi.org/10.5194/acp-13-4543-2013>, 2013.
- Carbajo, P. G. and Orr-Ewing, A. J.: NO₂ quantum yields from ultraviolet photodissociation of methyl and isopropyl nitrate, *Physical Chemistry Chemical Physics*, 12, 6084–6091, <https://doi.org/10.1039/c001425g>, 2010.
- 520 Clemetshaw, K. C., Williams, J., Rattigan, O. v., Shallcross, D. E., Law, K. S., and Anthony Cox, R.: Gas-phase ultraviolet absorption cross-sections and atmospheric lifetimes of several C₂–C₅ alkyl nitrates, *J Photochem Photobiol A Chem*, 102, 117–126, [https://doi.org/10.1016/S1010-6030\(96\)04458-9](https://doi.org/10.1016/S1010-6030(96)04458-9), 1997.
- Darer, A. I., Cole-Filipiak, N. C., O'Connor, A. E., and Elrod, M. J.: Formation and stability of atmospherically relevant isoprene-derived organosulfates and organonitrates, *Environ Sci Technol*, 45, 1895–1902, <https://doi.org/10.1021/es103797z>, 2011.
- 525 Fisher, J. A., Jacob, D. J., Travis, K. R., Kim, P. S., Marais, E. A., Miller, C. C., Yu, K., Zhu, L., Yantosca, R. M., Sulprizio, M. P., Mao, J., Wennberg, P. O., Crounse, J. D., Teng, A. P., Nguyen, T. B., Clair, J. M. S., Cohen, R. C., Romer, P., Nault, B. A., Wooldridge, P. J., Jimenez, J. L., Campuzano-Jost, P., Day, D. A., Hu, W., Shepson, P. B., Xiong, F., Blake, D. R., Goldstein, A. H., Misztal, P. K., Hanisco, T. F., Wolfe, G. M., Ryerson, T. B., Wisthaler, A., and Mikoviny, T.: Organic nitrate chemistry and its implications for nitrogen budgets in an isoprene- and monoterpene-rich atmosphere: Constraints from aircraft (SEAC4RS) and ground-based (SOAS) observations in the Southeast US, *Atmos Chem Phys*, 16, 5969–5991, <https://doi.org/10.5194/acp-16-5969-2016>, 2016.
- 530 González-Sánchez, J. M., Brun, N., Wu, J., Morin, J., Temime-Roussel, B., Ravier, S., Mouchel-Vallon, C., Clément, J.-L., and Monod, A.: On the importance of atmospheric loss of organic nitrates by aqueous-phase ·OH-oxidation, *Atmos Chem Phys*, 21, 4915–4937, <https://doi.org/10.5194/acp-2020-684>, 2021.
- Herrmann, H.: On the photolysis of simple anions and neutral molecules as sources of O-/OH, SO_x- and Cl in aqueous solution, <https://doi.org/10.1039/b618565g>, 23 July 2007.
- Hu, K. S., Darer, A. I., and Elrod, M. J.: Thermodynamics and kinetics of the hydrolysis of atmospherically relevant organonitrates and organosulfates, *Atmos Chem Phys*, 11, 8307–8320, <https://doi.org/10.5194/acp-11-8307-2011>, 2011.
- 540 Jacobs, M. I., Burke, W. J., and Elrod, M. J.: Kinetics of the reactions of isoprene-derived hydroxynitrates: Gas phase epoxide formation and solution phase hydrolysis, *Atmos Chem Phys*, 14, 8933–8946, <https://doi.org/10.5194/acp-14-8933-2014>, 2014.

- Jenkin, M. E., Valorso, R., Aumont, B., Rickard, A. R., and Wallington, T. J.: Estimation of rate coefficients and branching ratios for gas-phase reactions of OH with aliphatic organic compounds for use in automated mechanism construction, *Atmos Chem Phys*, 18, 9297–9328, <https://doi.org/10.5194/acp-18-9297-2018>, 2018.
- Kiendler-Scharr, A., Mensah, A. A., Friese, E., Topping, D., Nemitz, E., Prevot, A. S. H., Äijälä, M., Allan, J., Canonaco, F., Canagaratna, M., Carbone, S., Crippa, M., Dall'Osto, M., Day, D. A., de Carlo, P., di Marco, C. F., Elbern, H., Eriksson, A., Freney, E., Hao, L., Herrmann, H., Hildebrandt, L., Hillamo, R., Jimenez, J. L., Laaksonen, A., McFiggans, G., Mohr, C., O'Dowd, C., Otjes, R., Ovadnevaite, J., Pandis, S. N., Poulain, L., Schlag, P., Sellegri, K., Swietlicki, E., Tiitta, P., Vermeulen, A., Wahner, A., Worsnop, D., and Wu, H. C.: Ubiquity of organic nitrates from nighttime chemistry in the European submicron aerosol, *Geophys Res Lett*, 43, 7735–7744, <https://doi.org/10.1002/2016GL069239>, 2016.
- Madronich, S.: Photodissociation in the atmosphere: 1. Actinic flux and the effects of ground reflections and clouds, *J Geophys Res*, 92, 9740–9752, <https://doi.org/10.1029/jd092id08p09740>, 1987.
- Madronich, S. and Flocke, S.: *The Role of Solar Radiation in Atmospheric Chemistry*, Springer, Berlin, Heidelberg, 1–26, https://doi.org/10.1007/978-3-540-69044-3_1, 1999.
- Morin, J., Bedjanian, Y., and Romanias, M. N.: Kinetics and Products of the Reactions of Ethyl and *n*-Propyl Nitrates with OH Radicals, *Int J Chem Kinet*, 48, 822–829, <https://doi.org/10.1002/kin.21037>, 2016.
- Müller, J. F., Peeters, J., and Stavrou, T.: Fast photolysis of carbonyl nitrates from isoprene, *Atmos Chem Phys*, 14, 2497–2508, <https://doi.org/10.5194/acp-14-2497-2014>, 2014.
- Ng, N. L., Brown, S. S., Archibald, A. T., Atlas, E., Cohen, R. C., Crowley, J. N., Day, D. A., Donahue, N. M., Fry, J. L., Fuchs, H., Griffin, R. J., Guzman, M. I., Herrmann, H., Hodzic, A., Iinuma, Y., Kiendler-Scharr, A., Lee, B. H., Luecken, D. J., Mao, J., McLaren, R., Mutzel, A., Osthoff, H. D., Ouyang, B., Picquet-Varraut, B., Platt, U., Pye, H. O. T., Rudich, Y., Schwantes, R. H., Shiraiwa, M., Stutz, J., Thornton, J. A., Tilgner, A., Williams, B. J., and Zaveri, R. A.: Nitrate radicals and biogenic volatile organic compounds: Oxidation, mechanisms, and organic aerosol, *Atmos Chem Phys*, 17, 2103–2162, <https://doi.org/10.5194/acp-17-2103-2017>, 2017.
- Nguyen, T. B., Crounse, J. D., Teng, A. P., Clair, J. M. S., Paulot, F., Wolfe, G. M., and Wennberg, P. O.: Rapid deposition of oxidized biogenic compounds to a temperate forest, *Proc Natl Acad Sci U S A*, 112, E392–E401, <https://doi.org/10.1073/pnas.1418702112>, 2015.
- Nissenon, P., Dabdub, D., Das, R., Maurino, V., Minero, C., and Vione, D.: Evidence of the water-cage effect on the photolysis of NO₃⁻ and FeOH₂⁺. Implications of this effect and of H₂O₂ surface accumulation on photochemistry at the air-water interface of atmospheric droplets, *Atmos Environ*, 44, 4859–4866, <https://doi.org/10.1016/j.atmosenv.2010.08.035>, 2010.
- Perring, A. E., Pusede, S. E., and Cohen, R. C.: An observational perspective on the atmospheric impacts of alkyl and multifunctional nitrates on ozone and secondary organic aerosol, *Chem Rev*, 113, 5848–5870, <https://doi.org/10.1021/cr300520x>, 2013.

- Picquet-Varrault, B., Suarez-Bertoa, R., Duncianu, M., Cazaunau, M., Pangui, E., David, M., and Doussin, J. F.: Photolysis and oxidation by OH radicals of two carbonyl nitrates: 4-nitrooxy-2-butanone and 5-nitrooxy-2-pentanone, *Atmos Chem Phys*, 20, 487–498, <https://doi.org/10.5194/acp-20-487-2020>, 2020.
- Renard, P., Siekmann, F., Gandolfo, A., Socorro, J., Salque, G., Ravier, S., Quivet, E., Clément, J.-L. L., Traikia, M., Delort, A.-M. M., Voisin, D., Vuitton, V., Thissen, R., and Monod, A.: Radical mechanisms of methyl vinyl ketone oligomerization through aqueous phase OH-oxidation: On the paradoxical role of dissolved molecular oxygen, *Atmos Chem Phys*, 13, 6473–6491, <https://doi.org/10.5194/acp-13-6473-2013>, 2013.
- Rindelaub, J. D., McAvey, K. M., and Shepson, P. B.: The photochemical production of organic nitrates from α -pinene and loss via acid-dependent particle phase hydrolysis, *Atmos Environ*, 100, 193–201, <https://doi.org/10.1016/j.atmosenv.2014.11.010>, 2015.
- Rindelaub, J. D., Borca, C. H., Hostetler, M. A., Slade, J. H., Lipton, M. A., Slipchenko, L. v., and Shepson, P. B.: The acid-catalyzed hydrolysis of an α -pinene-derived organic nitrate: Kinetics, products, reaction mechanisms, and atmospheric impact, *Atmos Chem Phys*, 16, 15425–15432, <https://doi.org/10.5194/acp-16-15425-2016>, 2016.
- Roberts, J. M. and Fajer, R. W.: UV Absorption Cross Sections of Organic Nitrates of Potential Atmospheric Importance and Estimation of Atmospheric Lifetimes, *Environ Sci Technol*, 23, 945–951, <https://doi.org/10.1021/es00066a003>, 1989.
- Romer, P. S., Wooldridge, P. J., Crounse, J. D., Kim, M. J., Wennberg, P. O., Dibb, J. E., Scheuer, E., Blake, D. R., Meinardi, S., Brosius, A. L., Thames, A. B., Miller, D. O., Brune, W. H., Hall, S. R., Ryerson, T. B., and Cohen, R. C.: Constraints on Aerosol Nitrate Photolysis as a Potential Source of HONO and NO_x, *Environ Sci Technol*, 52, 13738–13746, <https://doi.org/10.1021/acs.est.8b03861>, 2018.
- Romer Present, P. S., Zare, A., and Cohen, R. C.: The changing role of organic nitrates in the removal and transport of NO_x, *Atmos Chem Phys*, 20, 267–279, <https://doi.org/10.5194/acp-20-267-2020>, 2020.
- Romonosky, D. E., Nguyen, L. Q., Shemesh, D., Nguyen, T. B., Epstein, S. A., Martin, D. B. C., Vanderwal, C. D., Gerber, R. B., and Nizkorodov, S. A.: Absorption spectra and aqueous photochemistry of β -hydroxyalkyl nitrates of atmospheric interest, *Mol Phys*, 113, 2179–2190, <https://doi.org/10.1080/00268976.2015.1017020>, 2015.
- Shen, H., Zhao, D., Pullinen, I., Kang, S., Vereecken, L., Fuchs, H., Acir, I. H., Tillmann, R., Rohrer, F., Wildt, J., Kiendler-Scharr, A., Wahner, A., and Mentel, T. F.: Highly Oxygenated Organic Nitrates Formed from NO₃ Radical-Initiated Oxidation of β -Pinene, *Environ Sci Technol*, 55, 15658–15671, <https://doi.org/10.1021/acs.est.1c03978>, 2021.
- Shepson, P. B.: Organic nitrates, Blackwell Publishing Ltd, Oxford, UK, 58–63 pp., <https://doi.org/10.1358/dnp.1999.12.1.863615>, 1999.
- Suarez-Bertoa, R., Picquet-Varrault, B., Tamas, W., Pangui, E., and Doussin, J. F.: Atmospheric fate of a series of carbonyl nitrates: Photolysis frequencies and OH-oxidation rate constants, *Environ Sci Technol*, 46, 12502–12509, <https://doi.org/10.1021/es302613x>, 2012.
- Svoboda, O., Kubelová, L., and Slavíček, P.: Enabling forbidden processes: Quantum and solvation enhancement of nitrate anion UV absorption, *Journal of Physical Chemistry A*, 117, 12868–12877, <https://doi.org/10.1021/jp4098777>, 2013.

- 610 Takeuchi, M. and Ng, N. L.: Chemical composition and hydrolysis of organic nitrate aerosol formed from hydroxyl and nitrate radical oxidation of α -pinene and β -pinene, *Atmos. Chem. Phys*, 19, 12749–12766, [https://doi.org/10.5194/acp-19-12749-](https://doi.org/10.5194/acp-19-12749-2019) 2019, 2019.
- Talukdar, R. K., Herndon, S. C., Burkholder, J. B., Roberts, J. M., and Ravishankara, A. R.: Atmospheric fate of several alkyl nitrates: Part 1. Rate coefficients of the reactions of alkyl nitrates with isotopically labelled hydroxyl radicals, *Journal of the* 615 *Chemical Society - Faraday Transactions*, 93, 2787–2796, <https://doi.org/10.1039/a701780d>, 1997a.
- Talukdar, R. K., Burkholder, J. B., Hunter, M., Gilles, M. K., Roberts, J. M., and Ravishankara, A. R.: Atmospheric fate of several alkyl nitrates: Part 2. UV absorption cross-sections and photodissociation quantum yields, *Journal of the Chemical Society - Faraday Transactions*, 93, 2797–2805, <https://doi.org/10.1039/a701781b>, 1997b.
- Tilgner, A., Bräuer, P., Wolke, R., and Herrmann, H.: Modelling multiphase chemistry in deliquescent aerosols and clouds 620 using CAPRAM3.0i, *J Atmos Chem*, 70, 221–256, <https://doi.org/10.1007/s10874-013-9267-4>, 2013.
- Wang, Y., Piletic, I. R., Takeuchi, M., Xu, T., France, S., and Ng, N. L.: Synthesis and Hydrolysis of Atmospherically Relevant Monoterpene-Derived Organic Nitrates, *Environ Sci Technol*, 55, 14595–14606, <https://doi.org/10.1021/acs.est.1c05310>, 2021.
- Wängberg, I., Barnes, I., and Becker, K. H.: Atmospheric chemistry of bifunctional cycloalkyl nitrates, *Chem Phys Lett*, 261, 625 138–144, [https://doi.org/10.1016/0009-2614\(96\)00857-3](https://doi.org/10.1016/0009-2614(96)00857-3), 1996.
- Warneck, P. and Wurzinger, C.: Product Quantum Yields for the 305-nm Photodecomposition of NO_3^- in Aqueous Solution, *J. Phys. Chem*, 6278–6283 pp., 1988.
- Zare, A., Fahey, K. M., Sarwar, G., Cohen, R. C., and Pye, H. O. T.: Vapor-Pressure Pathways Initiate but Hydrolysis Products Dominate the Aerosol Estimated from Organic Nitrates, *ACS Earth Space Chem*, 3, 1426–1437, 630 <https://doi.org/10.1021/acsearthspacechem.9b00067>, 2019.

Supplementary information to “On the importance of multiphase photolysis of organic nitrates on their global atmospheric removal”

Juan Miguel González-Sánchez^{1,2}, Nicolas Brun^{1,2}, Junteng Wu¹, Sylvain Ravier¹, Jean-Louis Clement², Anne Monod¹

¹Aix Marseille Univ, CNRS, LCE, Marseille, France

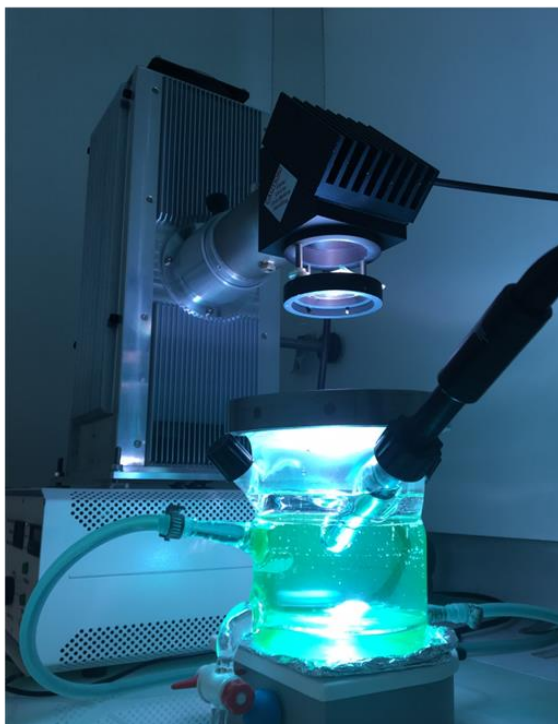
²Aix Marseille Univ, CNRS, LCE, Marseille, France

Correspondence to: Anne Monod (anne.monod@univ-amu.fr) and Juan Miguel González-Sánchez (juan.gonzalez@mio.osupytheas.fr)

Figure S1: Experimental setup used for the photolysis experiments.	3
Section S1: Actinometry study	4
Table S1.1: actinometry study using H ₂ O ₂ : initial conditions and experimentally determined aqueous-phase photolysis rate constants.	4
Section S2: Determination of the experimental photolysis rate constants of RONO ₂	6
Table S2.1: Chemical reactions contributing to the formation and consumption of ·OH radicals during RONO ₂ photolysis.	6
Table S2.2: RONO ₂ photolysis experiments: initial conditions and kinetic results.	7
Table S2.3: RONO ₂ control experiments: initial conditions and kinetic results.	7
Table S1. List of the investigated compounds for absorption cross-section determinations in water or methanol at wavelengths ranging from 190 to 600 nm.	8
Figure S2. Absorption spectra of various aqueous solutions of isosorbide 5-mononitrate (from 0.001 to 0.02 M). The embedded graph represents the same data between 290 to 340 nm, the actinic region relevant for atmospheric photolysis	9
Section S3: Synthesis of α -nitrooxyacetone and 1-nitrooxy-2-propanol	10
Figure S3.1. ¹ H-NMR spectra of α -nitrooxyacetone in CDCl ₃	10
Figure S3.2. ¹ H-NMR spectra of 1-nitrooxy-2-propanol in D ₂ O.	11
Section S4: Determination of the RONO ₂ liquid-phase absorption cross-sections	12
Figure S4.1. Determination of the aqueous-phase cross-sections of isosorbide 5-mononitrate at 300 nm between 0.001 to 0.02 M.	12
Table S2. Experimentally determined liquid-phase absorption cross-sections of RONO ₂	13

Section S5: Deconvolution of the absorption cross-section spectra of α -nitrooxyacetone to remove the band observed above 320 nm which may be due to an impurity	15
Figure S5.1. Deconvolution of the experimental absorption cross-sections of α -nitrooxyacetone into three absorption bands.....	15
Section S6. Methodology for Section 4 calculations.....	16
Section S6.1. Calculation of RONO_2 partitioning and assignment of aqueous and gas phase J and k_{OH} for RONO_2 in Section 4.1	16
Section S6.2. Assignment of J_{aq} and $k_{\text{OH, aq}}$ for RONO_2 in Section 4.2.....	16
Section S6.3. Assignment of dry and wet k_{dep} for RONO_2 in Section 4.3.....	17
Table S3. Atmospherically relevant non-hydrolyzable RONO_2 Henry's Law constants, aqueous-phase and gas-phase $\cdot\text{OH}$ -oxidation rate constants, aqueous-phase and gas-phase photolysis rate constants, molar fractions, and multiphase lifetimes at cloud/fog ($\text{LWC} = 0.35 \text{ g m}^{-3}$) and wet aerosol ($\text{LWC} = 3 \cdot 10^{-5} \text{ g m}^{-3}$) conditions.	18
Table S4. Atmospherically relevant hydrolyzable RONO_2 Henry's Law constants, aqueous-phase and gas-phase $\cdot\text{OH}$ -oxidation rate constants, aqueous-phase and gas-phase photolysis rate constants, and molar fractions and multiphase lifetimes at cloud/fog ($\text{LWC} = 0.35 \text{ g m}^{-3}$) and wet aerosol ($\text{LWC} = 3 \cdot 10^{-5} \text{ g m}^{-3}$) conditions.....	23
Table S5. Gas-phase photolysis rate constants and lifetimes for alkyl nitrates, dinitrates and carbonyl nitrates reported from the literature.	26
References	28

$\delta = 4 \text{ cm}$
(radius of the most intense spot)



$d = 18.4 \text{ cm}$
(radius between the lamp and
the water surface)

Figure S1: Experimental setup used for the photolysis experiments.

Section S1: Actinometry study

The lamp actinic flux that reaches the photoreactor was determined by performing an actinometry study with H_2O_2 .

In a first step, the lamplight spectra were measured in the most intense spot of the lamplight (with a radius $r = 2$ cm, Fig. S1) at a distance of $d = 18.2$ cm using a spectrophotometer.

In a second step, the theoretical aqueous-phase photolysis rate constant of H_2O_2 ($J_{H_2O_2,calc.}$, in s^{-1}) was calculated using Eq. (S1):

$$J_{H_2O_2,calc.} = \int \sigma_{H_2O_2}(\lambda) \cdot \Phi_{H_2O_2}(\lambda) \cdot I(\lambda)_{meas.} \cdot d\lambda, \quad (S1)$$

where $\sigma_{H_2O_2}(\lambda)$ is the aqueous-phase absorption cross-section values determined in this work (Table S2), $\Phi_{H_2O_2}(\lambda)$ is the recommended quantum yields values by Bianco et al., (2020), and $I(\lambda)_{meas.}$ is the lamp actinic flux measured in the first step. Using these data, one obtains an aqueous-phase H_2O_2 photolysis rate constant of $4.2 \times 10^{-5} s^{-1}$.

In a third step, the experimental photolysis rate constant of H_2O_2 ($J_{H_2O_2,exp.}$, in s^{-1}) was determined in the photoreactor during four photolysis experiments. The experimental protocol was the one used for $RONO_2$ photolysis experiments (described in Section 3.2), but experiments lasted 5 h instead of 7 h. The aqueous-phase concentration relative decay of H_2O_2 was monitored by offline UHPLC-UV analyses. During each photolysis experiment, H_2O_2 was consumed by its direct photolysis (RS1), but also by $\cdot OH$ radicals (RS2) formed through H_2O_2 photolysis. H_2O_2 is also regenerated via $HO_2\cdot/O_2^{\cdot-}$ self-reactions (RS3 and RS4).



Therefore, to account for all sources and sinks, the experimental H_2O_2 photolysis rate constant was determined using Eq. (S2):

$$\ln \frac{[H_2O_2]_0}{[H_2O_2]_t} = 2 \cdot J_{H_2O_2,exp.} \cdot t, \quad (S2)$$

where $[H_2O_2]_0/[H_2O_2]_t$ is the aqueous-phase concentration relative decay of H_2O_2 and t is the time (s). Equation (S2) is obtained by assuming steady-state of $\cdot OH$, $HO_2\cdot$, and $O_2^{\cdot-}$ radical concentrations. The determined aqueous-phase H_2O_2 photolysis rate constants of each photolysis experiment are compiled in Table S1 along with the initial conditions.

Table S1.1: actinometry study using H_2O_2 : initial conditions and experimentally determined aqueous-phase photolysis rate constants.

Exp.	$[H_2O_2]_0$ (mM)	$J_{H_2O_2,exp.}$ ($\times 10^{-6} s^{-1}$)
1	20.5	7.2 ± 0.2
2	21.0	8.1 ± 0.3
3	22.4	7.6 ± 0.7
4	19.8	6.9 ± 0.8
Average		7.5 ± 0.5

Finally, the ratio of $J_{H_2O_2,calc.}$ to $J_{H_2O_2,exp.}$ (Eq. S3) represents the correction factor (cf).

$$cf = \frac{J_{H_2O_2,calc.}}{J_{H_2O_2,exp.}} \quad (S3)$$

Multiplying the correction factor to the measured, $I(\lambda)_{meas.}$, one obtains the lamp actinic flux that reaches the photoreactor (Eq. S4).

$$I(\lambda)_{reac.} = cf \cdot I(\lambda)_{meas.} \quad (S4)$$

The correction factor was determined to be 5.6.

Section S2: Determination of the experimental photolysis rate constants of RONO₂

As discussed in Section 3.2, the decay of RONO₂ in each photolysis experiment was not only due to its photolysis. Other processes such as evaporation (for isopropyl nitrate and isobutyl nitrate), hydrolysis (α -nitrooxyacetone), and/or \cdot OH oxidation (for all) contribute to their decay. Therefore, the decay of RONO₂ is given by Eq. (S5) during each photolysis experiment:

$$\ln \frac{[\text{RONO}_2]_0}{[\text{RONO}_2]_t} = k' \cdot t = (J_{\text{RONO}_2} + k_{\text{vap/hyd}} + k_{\text{OH}}[\cdot \text{OH}]) \cdot t, \quad (\text{S5})$$

where k' (s⁻¹) is the experimental total decay rate constant of RONO₂ which shows a pseudo-first order behavior at the beginning of the reaction when the \cdot OH-oxidation contributes to less than 10 % of the total decay (first two hours of reaction); k_{vap} and k_{hyd} (s⁻¹) are the evaporation and hydrolysis rate constants and were determined during control experiments (Table S4); k_{OH} is the aqueous-phase \cdot OH-oxidation rate constant and was taken from González-Sánchez et al., (2021); $[\cdot \text{OH}]$ is the concentration of \cdot OH radicals and was estimated assuming steady-state concentrations (using Eq. (S6)):

$$[\cdot \text{OH}] = \frac{J_{\text{HNO}_2}[\text{HNO}_2] + J_{\text{NO}_2^-}[\text{NO}_2^-]}{k_{\text{OH,RONO}_2}[\text{RONO}_2] + k_{\text{OH,HNO}_2}[\text{HNO}_2] + k_{\text{OH,NO}_2^-}[\text{NO}_2^-]}, \quad (\text{S6})$$

where the photolysis rate constants of HNO₂ and NO₂⁻ (J_{HNO_2} and $J_{\text{NO}_2^-}$) were calculated using Eq. (S1), using absorption cross-sections from Fischer and Warneck, (1996); using quantum yields from Fischer and Warneck, (1996) for HNO₂ and from Herrmann, (2007) for NO₂⁻; and using the corrected lamp actinic flux. The total concentration of HNO₂ and NO₂⁻ (written [NO₂⁻]_T) was determined by High Pressure Ionic Chromatography measurements, and thus the concentration of each species was calculated using Eq. (S7) and Eq. (S8).

$$[\text{HNO}_2] = \frac{[\text{NO}_2^-]_T}{1 + K_a / 10^{-\text{pH}}} \quad (\text{S7})$$

$$[\text{NO}_2^-] = [\text{NO}_2^-]_T - [\text{HNO}_2], \quad (\text{S8})$$

where K_a is the acid dissociation constant of HNO₂, the pH was measured in all photolysis experiments (except during 1-nitrooxy-2-propanol photolysis experiments, for which average pH values were taken from the other experiments). Additionally, during α -nitrooxyacetone experiments, [NO₂⁻]_T was not measured and thus, average concentrations from other experiments were used instead. Table S2.1 lists the system of reactions that results in \cdot OH radical formation during RONO₂ photolysis with the corresponding reaction rate constants.

Table S2.1: Chemical reactions contributing to the formation and consumption of \cdot OH radicals during RONO₂ photolysis.

Reaction	K _a , J or k _{OH}	Ref.	N ^o
$\text{RONO}_2 + h\nu \rightarrow \text{R}'\text{O} + \text{HNO}_2$	J_{RONO_2}		RS5
$\text{HNO}_2 + \text{H}_2\text{O} \rightarrow \text{NO}_2^- + \text{H}_3\text{O}^+$	$K_a = 7.1 \cdot 10^{-4} \text{ M}$	a	RS6
$\text{NO}_2^- + h\nu \rightarrow \cdot \text{NO} + \cdot \text{O}^-$	$J = 5.8 \cdot 10^{-5} \text{ s}^{-1}$	a,b	RS7
$\text{HNO}_2 + h\nu \rightarrow \cdot \text{NO} + \cdot \text{OH}$	$J = 8.4 \cdot 10^{-4} \text{ s}^{-1}$	a,b	RS8
$\cdot \text{O}^- + \text{H}_3\text{O}^+ \leftrightarrow \cdot \text{OH} + \text{H}_2\text{O}$	$K_a = 2.8 \cdot 10^{-12} \text{ M}$	c	RS9
$\text{RONO}_2 + \cdot \text{OH} \rightarrow \text{products}$	$k_{\text{OH+RONO}_2}$	d	RS10
$\text{NO}_2^- + \cdot \text{OH} \rightarrow \cdot \text{NO}_2 + \text{OH}^-$	$k_{\text{OH}} = 1.0 \cdot 10^{10} \text{ M}^{-1} \text{ s}^{-1}$	a	RS11
$\text{HNO}_2 + \cdot \text{OH} \rightarrow \cdot \text{NO}_2 + \text{H}_2\text{O}$	$k_{\text{OH}} = 2.6 \cdot 10^9 \text{ M}^{-1} \text{ s}^{-1}$	a	RS12

^aFischer and Warneck, (1996). ^bHerrmann, (2007) ^cPoskrebsyshev et al., (2002) ^dGonzález-Sánchez et al., (2021).

Table S2.2 lists the initial conditions for each photolysis experiment and the results: k' is the experimental decay rate constant at the beginning of the reaction (< 2 h) and the corresponding photolysis rate constant.

Table S2.2: RONO2 photolysis experiments: initial conditions and kinetic results.

Exp.	RONO ₂	[RONO ₂] ₀	k' (x10 ⁻⁵ s ⁻¹)	J_{RONO_2} (x10 ⁻⁶ s ⁻¹)
1	Isopropyl nitrate	0.93	1.7	5.9
2	Isopropyl nitrate	1.81	1.4	5.1
3	Isopropyl nitrate	1.71	1.0	3.9
4	Isobutyl nitrate	0.60	2.9	13.7
5	Isobutyl nitrate	0.59	2.5	10.3
6	Isobutyl nitrate	0.53	1.9	7.0
7	Isobutyl nitrate	0.55	2.6	10.7
8	Isobutyl nitrate	0.49	1.4	5.0
9	α -Nitrooxyacetone	1.18	0.59	3.1
10	1-Nitrooxy-2-propanol	0.72	0.49	3.8
11	1-Nitrooxy-2-propanol	0.38	0.52	4.3

Table S2.3 lists the initial conditions for each control experiment where k_{vap} or k_{hyd} were experimentally determined using Eq. (S9). The protocol of these experiments is the same as the one used during the photolysis experiments (Section 2.2), but they were performed under dark conditions.

$$\ln \frac{[\text{RONO}_2]_0}{[\text{RONO}_2]_t} = k_{\text{vap/hyd}} \cdot t \quad (\text{S9})$$

Table S2.3: RONO2 control experiments: initial conditions and kinetic results.

Exp.	RONO ₂	[RONO ₂] ₀	k_{vap} (x10 ⁻⁶ s ⁻¹)	k_{hyd} (x10 ⁻⁶ s ⁻¹)
1	Isopropyl nitrate	0.84	9.7	–
2	Isopropyl nitrate	1.72	8.8	–
3	Isopropyl nitrate	1.66	5.6	–
4	Isopropyl nitrate	1.71	7.3	–
5	Isopropyl nitrate	1.82	6.5	–
6	Isobutyl nitrate	0.60	20.1	–
7	Isobutyl nitrate	0.52	8.1	–
8	Isobutyl nitrate	0.57	10.6	–
9	Isobutyl nitrate	0.57	20.8	–
10	α -Nitrooxyacetone	1.27	–	1.7
11	1-Nitrooxy-2-propanol	0.99	–	–
12	1-Nitrooxy-2-propanol	0.90	–	–
14	1-Nitrooxy-2-propanol	0.80	–	–

Table S1. List of the investigated compounds for absorption cross-section determinations in water or methanol at wavelengths ranging from 190 to 600 nm.

RONO₂	[RONO₂]₀ (mM)	Solvent
Isopropyl nitrate	0.5 – 2	H ₂ O
Isopropyl nitrate	1 – 10	CH ₃ OH
Isobutyl nitrate	1 – 10	CH ₃ OH
1-Pentyl nitrate	1 – 20	CH ₃ OH
Isopentyl nitrate	1 – 20	CH ₃ OH
2-Ethylhexyl nitrate	2 – 20	CH ₃ OH
α -Nitrooxyacetone	1 – 20	H ₂ O/CH ₃ OH (50/50, v/v)
1-Nitrooxy-2-propanol	1 – 10	H ₂ O
Isosorbide 5-mononitrate	1 – 20	H ₂ O
H ₂ O ₂	1 – 25	H ₂ O

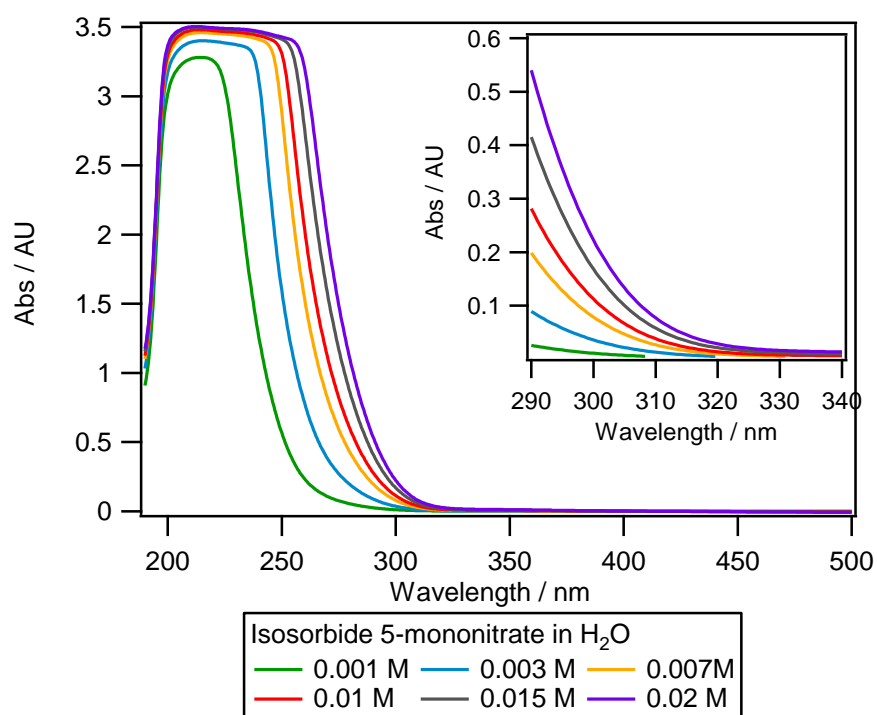


Figure S2. Absorption spectra of various aqueous solutions of isosorbide 5-mononitrate (from 0.001 to 0.02 M). The embedded graph represents the same data between 290 to 340 nm, the actinic region relevant for atmospheric photolysis

Section S3: Synthesis of α -nitrooxyacetone and 1-nitrooxy-2-propanol

α -Nitrooxyacetone 1.2 eq-mol of KI (98%, Sigma Aldrich) was added to a solution of chloroacetone (95%, Sigma Aldrich) in acetone. The solution was stirred in the dark at room temperature for 20 h. The mixture was filtered and concentrated under vacuum. The crude mixture was purified by silica gel column chromatography (pentane 10:1 ethyl acetate) leading to a deep brown oil. To an acetonitrile solution of iodoacetone, 1.5 eq-mol of AgNO_3 (99%, VWR Chemicals) was slowly added under dark conditions at 0 °C and stirred for 20 h at room temperature (under dark conditions). The precipitate was filtered and concentrated under vacuum. The crude mixture was purified by silica gel column chromatography (pentane 1:1 ethyl acetate) and lead to a yellow oil. $^1\text{H-NMR}$ (300 MHz, CDCl_3) δ : 2.24 (3H, s) 4.95 (2H, s). MS (EI): m/z : 43 (CH_3CO^+), 46 (NO_2^+), 57 ($\text{CH}_3\text{COCH}_2^+$), 76 ($\text{CH}_2\text{ONO}_2^+$).

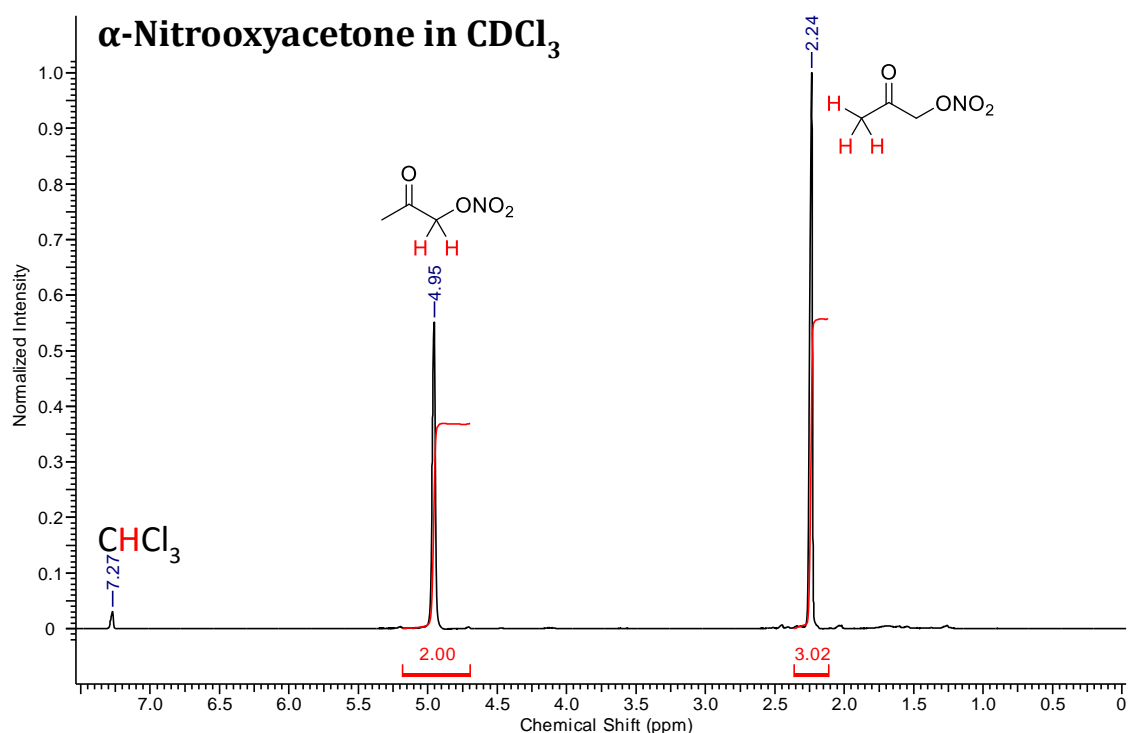


Figure S3.1. $^1\text{H-NMR}$ spectra of α -nitrooxyacetone in CDCl_3 .

1-Nitrooxy-2-propanol. 0.4 eq-mol of NaBH_4 (98%, Sigma Aldrich) and a 0.2 eq-mol NaHCO_3 (99.7%, Sigma Aldrich) were added to a solution of α -nitrooxyacetone in ethanol at 0 °C. The mixture was stirred at room temperature for 4 hours, concentrated under vacuum, and purified by silica gel column chromatography (pentane 3:1 ethyl acetate) to lead to a transparent oil. $^1\text{H-NMR}$ (300 MHz, D_2O) δ : 1.23 (3H, d, 6 Hz), 4.17 (1H, m), 4.42 (1H, m), 4.57 (1H, m). MS (EI): m/z : 45 ($\text{CH}_3\text{CH}(\text{OH})^+$), 46 (NO_2^+), 59 ($\text{CH}_3\text{CH}(\text{OH})\text{CH}_2^+$), 76 ($\text{CH}_2\text{ONO}_2^+$).

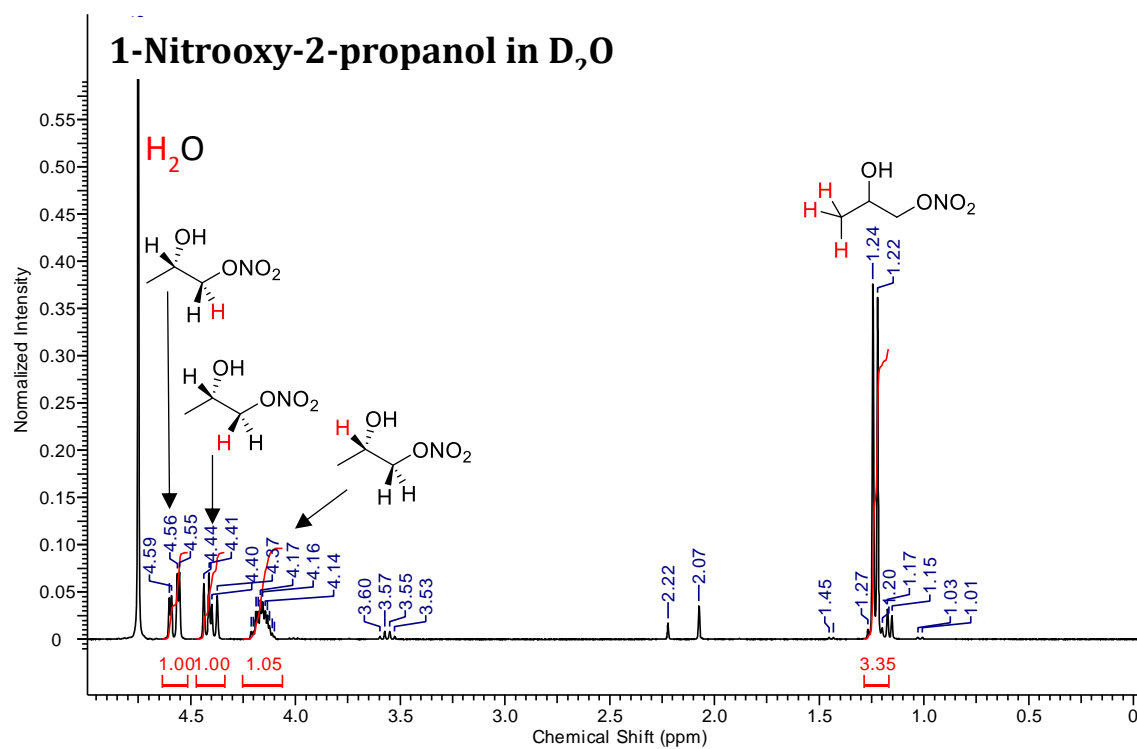


Figure S3.2. ¹H-NMR spectra of 1-nitrooxy-2-propanol in D₂O.

Section S4: Determination of the RONO₂ liquid-phase absorption cross-sections

The absorption cross-sections of each investigated compound were determined using Eq. (2):

$$Abs(\lambda) \cdot \ln 10 = \sigma(\lambda) \cdot L \cdot N, \quad (2)$$

where $Abs(\lambda)$ is the light absorbance of each RONO₂ at a determined wavelength, σ is the absorption cross-section of the molecule (in cm² molec.⁻¹) at a determined wavelength, N is the density of the molecule (molec. cm⁻³), and L is the absorption path length (cm). By plotting $Abs \cdot \ln 10$ versus $L \cdot N$ one obtains a straight line with slope = $\sigma(\lambda)$ and the intercept at the origin.

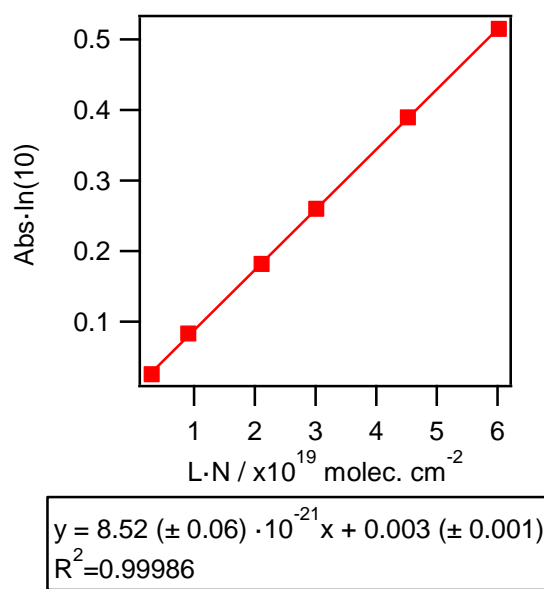


Figure S4.1. Determination of the aqueous-phase cross-sections of isosorbide 5-mononitrate at 300 nm between 0.001 to 0.02 M.

For each RONO₂, the absorption cross-sections between 290 to 340 nm were determined in the liquid phase (water or methanol). Absorbances were corrected by subtracting the signal measured between 360 to 500 nm (a region where no absorption occurs). An example of the determination of a cross-section value is given in Fig. S5. Although the methodology is simple, the presence of impurities with absorbing properties can entail significant deviations in the determination. Both α -nitrooxyacetone and 1-nitrooxy-2-propanol were synthesized and purified by a chromatographic column (Section S3). Despite this purification, small impurities were still suspected for both compounds, and thus the results obtained for these two compounds should be considered carefully.

Table S2. Experimentally determined liquid-phase absorption cross-sections of RONO₂.

RONO ₂	Isopropyl nitrate	Isopropyl nitrate	Isobutyl nitrate	1-Pentyl nitrate	Isopentyl nitrate	2- Ethylhexy l nitrate	α - Nitrooxy- acetone	1-Nitrooxy- 2-propanol	Isosorbide 5- mononitrate
Solvent	Water	Methanol	Methanol	Methanol	Methanol	Methanol	Me/Wa*	Water	Water
Wavelength / nm	σ ($\cdot 10^{-20}$ cm ² molec. ⁻¹)	σ ($\cdot 10^{-20}$ cm ² molec. ⁻¹)	σ ($\cdot 10^{-20}$ cm ² molec. ⁻¹)	σ ($\cdot 10^{-20}$ cm ² molec. ⁻¹)	σ ($\cdot 10^{-20}$ cm ² molec. ⁻¹)	σ ($\cdot 10^{-20}$ cm ² molec. ⁻¹)	σ ($\cdot 10^{-20}$ cm ² molec. ⁻¹)	σ ($\cdot 10^{-20}$ cm ² molec. ⁻¹)	σ ($\cdot 10^{-20}$ cm ² molec. ⁻¹)
290	1.95	1.98	2.19	2.29	2.34	12.17	3.03	2.07	1.98
292	1.69	1.77	1.91	1.99	2.05	10.97	2.67	1.76	1.77
294	1.44	1.57	1.65	1.71	1.79	9.90	2.33	1.49	1.57
296	1.22	1.38	1.42	1.46	1.55	8.97	2.03	1.25	1.38
298	1.03	1.20	1.21	1.24	1.34	8.17	1.77	1.03	1.20
300	0.86	1.04	1.02	1.04	1.14	7.47	1.53	0.85	1.04
302	0.70	0.90	0.85	0.86	0.97	6.87	1.32	0.70	0.90
304	0.58	0.77	0.71	0.70	0.81	6.36	1.14	0.57	0.77
306	0.46	0.66	0.58	0.57	0.68	5.94	0.99	0.46	0.66
308	0.37	0.55	0.47	0.46	0.57	5.60	0.85	0.37	0.55
310	0.29	0.46	0.38	0.37	0.47	5.33	0.74	0.29	0.46
312	0.23	0.39	0.31	0.29	0.39	5.12	0.65	0.24	0.39
314	0.17	0.32	0.25	0.22	0.33	4.98	0.57	0.19	0.32
316	0.13	0.27	0.20	0.16	0.27	4.87	0.51	0.16	0.27
318	0.10	0.22	0.16	0.12	0.23	4.80	0.46	0.13	0.22
320	0.08	0.19	0.13	0.09	0.20	4.76	0.41	0.11	0.19
322	0.06	0.15	0.10	0.06	0.17	4.74	0.38	0.09	0.15
324	0.04	0.13	0.09	0.04	0.15	4.74	0.35	0.08	0.13
326	0.03	0.11	0.07	0.03	0.13	4.73	0.33	0.07	0.11
328	0.03	0.09	0.06	0.02	0.12	4.72	0.31	0.07	0.09
330	0.02	0.07	0.06	0.01	0.11	4.72	0.29	0.06	0.07
332	0.02	0.06	0.05		0.10	4.72	0.28	0.06	0.06
334	0.02	0.05	0.05		0.10	4.72	0.26	0.06	0.05
336	0.01	0.04	0.04		0.09	4.69	0.25	0.06	0.04
338	0.01	0.04	0.04		0.09	4.64	0.24	0.05	0.04
340	0.01	0.03	0.04		0.08	4.58	0.23	0.05	0.03
345						4.39			
350						4.04			
355						3.59			
360						3.07			
365						2.51			
370						1.97			

375	1.52
380	1.13
385	0.84
390	0.62

***Methanol/Water (50/50, v/v)**

Section S5: Deconvolution of the absorption cross-section spectra of α -nitrooxyacetone to remove the band observed above 320 nm which may be due to an impurity

To remove the band observed above 320 nm, the absorption cross-sections of α -nitrooxyacetone were deconvoluted into three gaussians by performing the fit of Eq. (S10) in our data.

$$f(x) = A_1 e^{-\frac{(x-b_1)^2}{2 \cdot c_1^2}} + A_2 e^{-\frac{(x-b_2)^2}{2 \cdot c_2^2}} + A_3 e^{-\frac{(x-b_3)^2}{2 \cdot c_3^2}} \quad (\text{S10})$$

with initial guesses of $2 \cdot 10^{-18}$, 205, and 28 for A_1 , b_1 , and c_1 , corresponding to the typical intense band of nitrooxy groups with a maximum at around 205 nm; of $6 \cdot 10^{-20}$, 270, and 20 for A_2 , b_2 , and c_2 , corresponding to the carbonyl group band with a maximum at around 270 nm; and of $4.5 \cdot 10^{-20}$, 340, and 250 for A_3 , b_3 , and c_3 , corresponding to the band observed above 320 nm and may potentially originate from an impurity.

Once the fit was calculated, the alternative absorption cross-sections of α -nitrooxyacetone in condensed phases was calculated by adding the first two gaussians. Using this absorption cross-section, a quantum yield average of 0.02 was calculated.

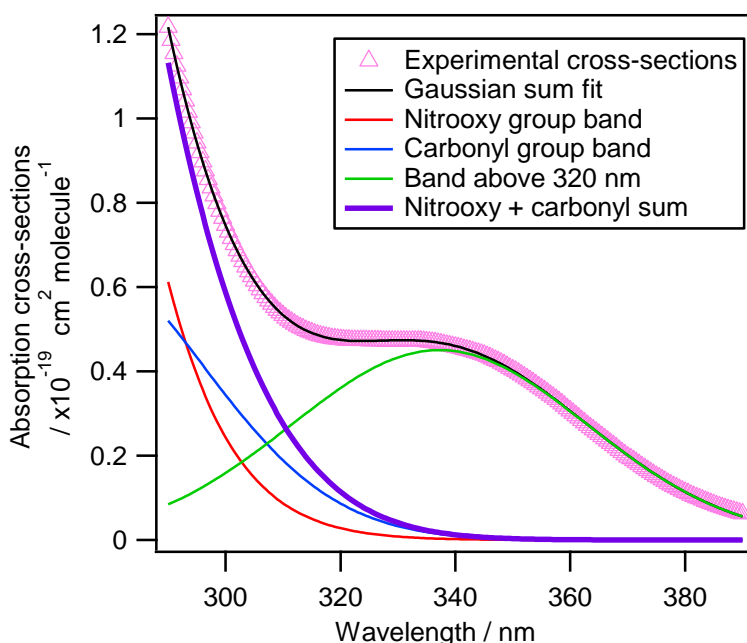


Figure S5.1. Deconvolution of the experimental absorption cross-sections of α -nitrooxyacetone into three absorption bands.

Section S6. Methodology for Section 4 calculations

Section S6.1. Calculation of RONO₂ partitioning and assignment of aqueous and gas phase J and k_{OH} for RONO₂ in Section 4.1

Partitioning. The partitioning of each molecule in the aqueous phase was calculated using Eq. (S10):

$$\varphi_{aq} = \frac{n_{aq}}{n_{aq} + n_{gas}} = \frac{1}{1 + (1/LWC_p \cdot K_H \cdot R \cdot T)}, \quad (S10)$$

where φ_{aq} is the molar fraction of the compound in the aqueous phase, n_{aq} and n_{gas} are the number of moles of RONO₂ in the aqueous and the gas phase, respectively; K_H is the Henry's Law constant at standard conditions (in M atm⁻¹); R is the ideal gas constant (0.082 atm L mol⁻¹ K⁻¹); T is the temperature (set at 298 K) and LWC_p is the liquid water content in volume units (m³ of water/m³ of air). Experimental K_H values were taken from (Sander, 2015) when available, or they were calculated using the GROHME method (Raventos-Duran et al., 2010).

·OH oxidation rate constants. Experimental values were used for $k_{OH,aq}$ and $k_{OH,gas}$ when available or they were calculated using the group contribution methods presented in González-Sánchez et al., (2021) and Jenkin et al., (2018), respectively.

Photolysis rate constants. J_{aq} and J_{gas} were calculated as described in Section 3 when experimental aqueous or gas-phase absorption cross-sections were available. When not available, average values were employed according to the molecule's chemical structure. For all investigated RONO₂, a unique J_{aq} value of $3.9 \cdot 10^{-7} \text{ s}^{-1}$ was considered. This value is the average of eight RONO₂ molecules bearing a carbonyl or a hydroxy group: α -nitrooxyacetone, 1-nitrooxy-2-propanol, isosorbide 5-mononitrate, and compounds A, B, C, D, and F in Table 2. This value is likely a good approximation since all the RONO₂ photolysis rate constants determined in this work fall in the same order of magnitude and do not present significant deviations (Table 2). For RONO₂ with undetermined gas-phase absorption cross-sections, three J_{gas} values were used depending on their chemical structure. A high value ($6.6 \cdot 10^{-5} \text{ s}^{-1}$) was used for carbonyl nitrates since these compounds present an enhancement in their photolysis rates compared to alkyl nitrates. This value was averaged from all carbonyl nitrates J_{gas} values available in the literature (see Table S5). For the C₅ dihydroxy dinitrate compound, a value of $4.4 \cdot 10^{-6} \text{ s}^{-1}$ was chosen, averaged from dinitrates photolysis rate constants. For other RONO₂, a value of $7.6 \cdot 10^{-7} \text{ s}^{-1}$ was chosen, averaged from photolysis rate constants of alkyl nitrates with more than 2 carbon atoms.

Section S6.2. Assignment of J and k_{OH} for RONO₂ in Section 4.2

The aqueous phase and gas phase photolysis and ·OH-oxidation rate constants were assumed or estimated as described in Section S6.1. Nevertheless, eight of the investigated molecules (all the allylic RONO₂ and tert 1, 2, 5, and 6) bear an unsaturation in their chemical structure, and thus their aqueous-phase ·OH-oxidation rate constant cannot be calculated with the Structure-Activity Relationship (SAR). For these compounds, a rate constant of $10^{10} \text{ M}^{-1} \text{ s}^{-1}$ was assumed. This assumption is based on the high reactivities (close to the diffusion limit) of unsaturated molecules due the ·OH addition on the double bond (Herrmann et al., 2015). Besides, it should be noted that no experimental photolysis rate constants were reported for allylic RONO₂ in any phase. Hence, the assumed photolysis rate constants have to be taken with caution.

Section S6.3. Assignment of dry and wet k_{dep} for RONO_2 in Section 4.3

Dry deposition rate constants were calculated considering a boundary height layer of 1000 m. The average daytime deposition velocities were assigned based on the chemical structure of the RONO_2 . For alkyl nitrates, a value of 0.15 cm s^{-1} (averaged from values determined by Abeleira et al., (2018) for RONO_2 bearing three to five carbon atoms). For terpene nitrates, a value of 0.8 cm s^{-1} was assumed (corresponding to the value determined by Nguyen et al., (2015) for two terpene nitrates). For the rest of RONO_2 , i.e., polyfunctional RONO_2 bearing less than 10 carbon atoms, a value of 1.5 cm s^{-1} was assumed (averaged from values determined by Nguyen et al., (2015) for four isoprene nitrates).

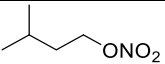
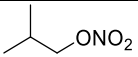
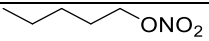
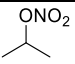
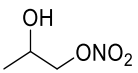
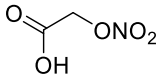
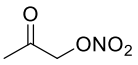
Wet deposition lifetimes were estimated from Brimblecombe and Dawson, (1984) using Eq. (S11):

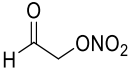
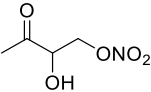
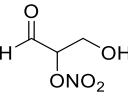
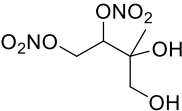
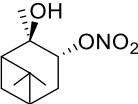
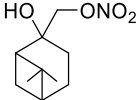
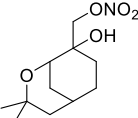
$$k_{wd} = \frac{R_r E e^{-z/H_x}}{H_x((K_H R T^{-1}) + L_{WC})}, \quad (\text{S11})$$

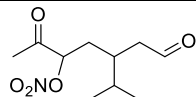
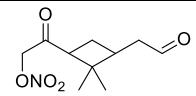
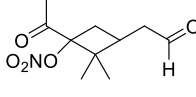
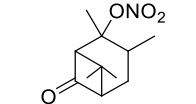
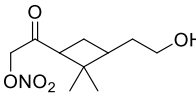
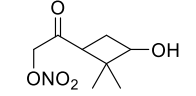
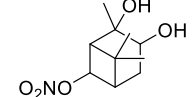
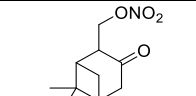
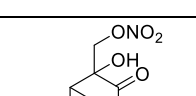
where k_{wd} is the wet deposition rate constant (in s^{-1}), R_r is the assumed annual rainfall rate ($3.17 \times 10^{-8} \text{ m s}^{-1}$ or 1 m yr^{-1}), E is the enhancement due to droplet evaporation (set at 1.33), z is the characteristic height for clouds (set at 3500 m), H_x is the scale height for the molecules (set at 2200 m), and L_{WC} is the liquid water content of the cloud ($3.5 \times 10^{-7} \text{ m}^3$ of water/ m^3 of air).

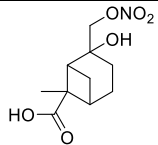
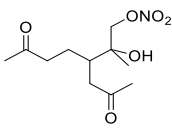
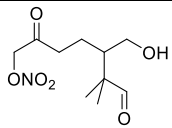
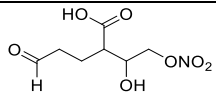
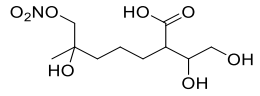
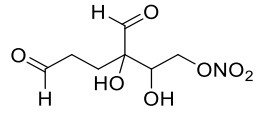
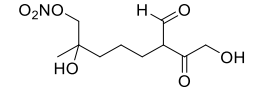
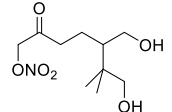
Since the rainfall rate is assumed yearly, wet deposition rate constants are considered equal in both cloud/fog and wet aerosol scenarios.

Table S3. Atmospherically relevant non-hydrolyzable RONO₂ Henry's Law constants, aqueous-phase and gas-phase ·OH-oxidation rate constants, aqueous-phase and gas-phase photolysis rate constants, molar fractions, and multiphase lifetimes at cloud/fog (LWC = 0.35 g m⁻³) and wet aerosol (LWC = 3 ·10⁻⁵ g m⁻³) conditions.

Small RONO ₂										
RONO ₂ structure	Name	K _H (M atm ⁻¹)	k _{OH, aq} (M ⁻¹ s ⁻¹)	k _{OH, gas} (cm ³ molec. ⁻¹ s ⁻¹)	J _{aq} (s ⁻¹)	J _{gas} (s ⁻¹)	Cloud/fog conditions (LWC = 0.35 g m ⁻³)		Wet aerosol conditions (LWC = 3 × 10 ⁻⁵ g m ⁻³)	
							φ _{aq} (%)	τ _{mult} (h)	φ _{aq} (%)	τ _{mult} (h)
	Isopentyl nitrate	0.45	2.22 × 10 ⁹	2.37 × 10 ⁻¹²	4.90 × 10 ⁻⁷	7.57 × 10 ⁻⁷	0.0	50	0.0	50
	Isobutyl nitrate	0.54	1.74 × 10 ⁹	1.43 × 10 ⁻¹²	5.90 × 10 ⁻⁷	5.25 × 10 ⁻⁷	0.0	69	0.0	69
	1-Pentyl nitrate	0.60	3.11 × 10 ⁹	3.13 × 10 ⁻¹²	3.04 × 10 ⁻⁷	8.89 × 10 ⁻⁷	0.0	41	0.0	41
	Isopropyl nitrate	0.62	2.84 × 10 ⁸	3.48 × 10 ⁻¹³	3.21 × 10 ⁻⁷	8.66 × 10 ⁻⁷	0.0	97	0.0	97
	1-Nitrooxy-2-propanol	1.10 × 10 ⁴	8.72 × 10 ⁸	5.10 × 10 ⁻¹²	4.20 × 10 ⁻⁷	4.88 × 10 ⁻⁹	5.4	12	0.0	12
	Nitrooxyacetic acid	1.62 × 10 ⁵	2.65 × 10 ⁷	5.99 × 10 ⁻¹²	3.95 × 10 ⁻⁷	7.57 × 10 ⁻⁷	58.1	12	0.0	12
Isoprene nitrates										
RONO ₂ structure	Name	K _H (M atm ⁻¹)	k _{OH, aq} (M ⁻¹ s ⁻¹)	k _{OH, gas} (cm ³ molec. ⁻¹ s ⁻¹)	J _{aq} (s ⁻¹)	J _{gas} (s ⁻¹)	Cloud/fog conditions (LWC = 0.35 g m ⁻³)		Wet aerosol conditions (LWC = 3 × 10 ⁻⁵ g m ⁻³)	
							φ _{aq} (%)	τ _{mult} (h)	φ _{aq} (%)	τ _{mult} (h)
	α-Nitrooxyacetone	1.01 × 10 ³	7.91 × 10 ⁷	4.33 × 10 ⁻¹³	5.51 × 10 ⁻⁸	1.29 × 10 ⁻⁵	0.9	9	0.0	9

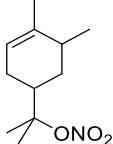
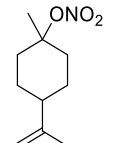
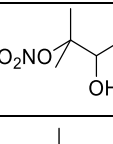
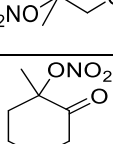
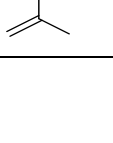
	Ethanal nitrate	6.17×10^3	5.53×10^8	7.44×10^{-12}	3.95×10^{-7}	6.15×10^{-5}	5.0	3	0.0	3
	Methyl vinyl ketone nitrate' (MVKN')	9.55×10^4	2.99×10^8	2.47×10^{-12}	3.95×10^{-7}	1.45×10^{-5}	45.0	9	0.0	7
	Methyl vinyl ketone nitrate (MVKN)	1.86×10^5	5.38×10^8	3.89×10^{-12}	3.95×10^{-7}	2.55×10^{-5}	61.4	7	0.0	5
	C ₅ dihydroxy dinitrate	8.71×10^7	1.12×10^9	8.36×10^{-12}	3.95×10^{-7}	4.42×10^{-6}	99.9	7	6.0	7
Terpene nitrates										
RONO ₂ structure	Name	K _H (M atm ⁻¹)	k _{OH, aq} (M ⁻¹ s ⁻¹)	k _{OH, gas} (cm ³ molec. ⁻¹ s ⁻¹)	J _{aq} (s ⁻¹)	J _{gas} (s ⁻¹)	Cloud/fog conditions (LWC = 0.35 g m ⁻³)		Wet aerosol conditions (LWC = 3 × 10 ⁻⁵ g m ⁻³)	
							φ _{aq} (%)	τ _{mult} (h)	φ _{aq} (%)	τ _{mult} (h)
	α-pinene 1	8.32×10^3	2.83×10^9	6.56×10^{-12}	3.95×10^{-7}	7.57×10^{-7}	6.6	14	0.0	15
	β-pinene 1	8.71×10^3	3.91×10^9	9.23×10^{-12}	3.95×10^{-7}	7.57×10^{-7}	6.9	11	0.0	12
	β-pinene 2	5.62×10^5	2.99×10^9	2.04×10^{-11}	3.95×10^{-7}	7.57×10^{-7}	82.8	6	0.0	6

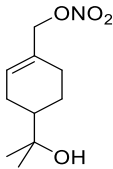
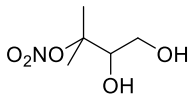
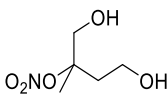
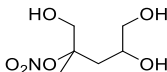
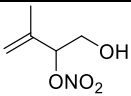
	γ -terpinen 1	1.02×10^6	5.46×10^9	3.50×10^{-11}	3.95×10^{-7}	6.57×10^{-5}	89.8	4	0.1	2
	β -pinen 3	3.72×10^6	4.22×10^9	2.87×10^{-11}	3.95×10^{-7}	6.57×10^{-5}	97.0	4	0.3	2
	α -pinen 2	4.57×10^6	3.56×10^9	2.66×10^{-11}	3.95×10^{-7}	6.57×10^{-5}	97.5	5	0.3	2
	α -pinen 3	2.34×10^7	1.78×10^9	6.21×10^{-12}	3.95×10^{-7}	7.57×10^{-7}	99.5	7	1.7	10
	β -pinen 4	3.98×10^7	4.54×10^9	1.12×10^{-11}	3.95×10^{-7}	6.57×10^{-5}	99.7	4	2.8	3
	β -pinen 5	5.01×10^7	2.48×10^9	8.63×10^{-12}	3.95×10^{-7}	6.57×10^{-5}	99.8	6	3.5	3
	α -pinen 4	2.24×10^8	2.50×10^9	2.23×10^{-11}	3.95×10^{-7}	7.57×10^{-7}	100.0	6	14.1	6
	β -pinen 6	2.95×10^8	2.64×10^9	1.34×10^{-11}	3.95×10^{-7}	6.57×10^{-5}	100.0	6	17.8	3
	β -pinen 7	1.32×10^9	2.47×10^9	6.56×10^{-12}	3.95×10^{-7}	6.57×10^{-5}	100.0	6	49.2	4

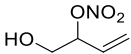
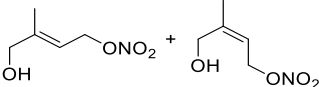
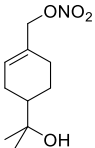
	β -pinen 8	3.39×10^9	3.54×10^9	1.39×10^{-11}	3.95×10^{-7}	7.57×10^{-7}	100.0	5	71.3	6
	limonen 1	1.12×10^{10}	4.00×10^9	4.58×10^{-11}	3.95×10^{-7}	7.57×10^{-7}	100.0	5	89.1	4
	β -pinen 9	3.39×10^{10}	6.20×10^9	5.49×10^{-11}	3.95×10^{-7}	6.57×10^{-5}	100.0	3	96.1	3
	myrcen 1	4.37×10^{10}	3.49×10^9	3.70×10^{-11}	3.95×10^{-7}	7.57×10^{-7}	100.0	5	97.0	5
	myrcen 2	4.90×10^{10}	5.41×10^9	2.55×10^{-11}	3.95×10^{-7}	7.57×10^{-7}	100.0	4	97.3	4
	myrcen 3	7.41×10^{10}	2.85×10^9	4.86×10^{-11}	3.95×10^{-7}	7.57×10^{-7}	100.0	6	98.2	6
	myrcen 4	2.34×10^{11}	4.79×10^9	4.05×10^{-11}	3.95×10^{-7}	7.57×10^{-7}	100.0	4	99.4	4
	β -pinen 10	3.24×10^{11}	6.43×10^9	2.01×10^{-11}	3.95×10^{-7}	6.57×10^{-5}	100.0	3	99.6	3

	β -pinen 11	4.17×10^{12}	4.55×10^9	2.45×10^{-11}	3.95×10^{-7}	6.57×10^{-5}	100.0	4	100.0	4
---	-------------------	-----------------------	--------------------	------------------------	-----------------------	-----------------------	-------	---	-------	---

Table S4. Atmospherically relevant hydrolyzable RONO₂ Henry's Law constants, aqueous-phase and gas-phase ·OH-oxidation rate constants, aqueous-phase and gas-phase photolysis rate constants, and molar fractions and multiphase lifetimes at cloud/fog (LWC = 0.35 g m⁻³) and wet aerosol (LWC = 3 ·10⁻⁵ g m⁻³) conditions.

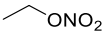
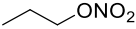
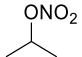
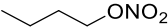
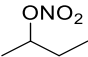
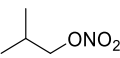
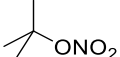
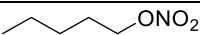
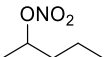
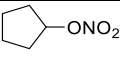
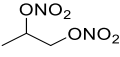
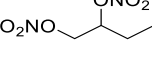
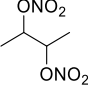
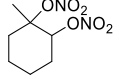
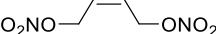
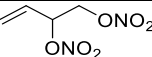
Tertiary RONO ₂											
Chemical structure	Name	K _H (M atm ⁻¹)	k _{hyd} (s ⁻¹)	k _{OH, aq} (M ⁻¹ s ⁻¹)	k _{OH, gas} (cm ³ molec. ⁻¹ s ⁻¹)	J _{aq} (s ⁻¹)	J _{gas} (s ⁻¹)	Cloud/fog conditions		Wet aerosol conditions	
								φ _{aq} (%)	τ _{mult} (h)	φ _{aq} (%)	τ _{mult} (h)
	tert 1 ^a	1.3	3.2 × 10 ⁻⁵	1.00 × 10 ¹⁰	9.90 × 10 ⁻¹¹	3.95 × 10 ⁻⁷	7.57 × 10 ⁻⁷	0.0	2	0.0	2
	tert 2 ^b	1.7	9.2 × 10 ⁻⁴	1.00 × 10 ¹⁰	6.58 × 10 ⁻¹¹	3.95 × 10 ⁻⁷	7.57 × 10 ⁻⁷	0.0	3	0.0	3
	tert 3 ^c	2.0 × 10 ³	9.3 × 10 ⁻³	7.07 × 10 ⁸	2.40 × 10 ⁻¹²	3.95 × 10 ⁻⁷	7.57 × 10 ⁻⁷	1.7	2	0.0	14
	tert 4 ^c	2.6 × 10 ³	9.3 × 10 ⁻³	5.54 × 10 ⁸	1.17 × 10 ⁻¹²	3.95 × 10 ⁻⁷	7.57 × 10 ⁻⁷	2.2	1	0.0	16
	tert 5 ^b	4.6 × 10 ³	3.7 × 10 ⁻⁵	1.00 × 10 ¹⁰	6.87 × 10 ⁻¹¹	3.95 × 10 ⁻⁷	6.57 × 10 ⁻⁵	3.8	2	0.0	2

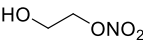
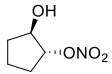
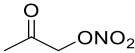
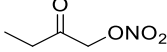
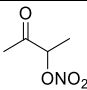
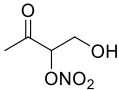
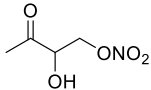
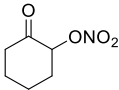
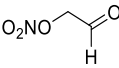
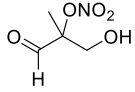
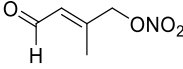
	tert 6 ^b	5.6×10^4	1.1×10^{-4}	1.00×10^{10}	1.72×10^{-10}	3.95×10^{-7}	7.57×10^{-7}	32.5	1	0.0	1
	tert 7 ^d	3.6×10^6	2.3×10^{-3}	1.11×10^9	1.28×10^{-11}	3.95×10^{-7}	7.57×10^{-7}	96.9	0.1	0.3	5
	tert 8 ^d	5.0×10^6	4.6×10^{-3}	2.27×10^9	5.71×10^{-12}	3.95×10^{-7}	7.57×10^{-7}	97.7	0.1	0.4	5
	tert 9 ^d	2.1×10^{10}	4.1×10^{-4}	1.39×10^9	2.91×10^{-11}	3.95×10^{-7}	7.57×10^{-7}	100.0	0.6	94.0	0.6
Allylic RONO ₂											
Chemical structure	Name	K_H (M atm ⁻¹)	k_{hyd} (s ⁻¹)	$k_{OH, aq}$ (M ⁻¹ s ⁻¹)	$k_{OH, gas}$ (cm ³ molec. ⁻¹ s ⁻¹)	J_{aq} (s ⁻¹)	J_{gas} (s ⁻¹)	Cloud/fog conditions		Wet aerosol conditions	
								φ_{aq} (%)	τ_{mult} (h)	φ_{aq} (%)	τ_{mult} (h)
	ally 1 ^e	8.3×10^3	1.6×10^{-5}	1.00×10^{10}	3.90×10^{-11}	3.95×10^{-7}	7.57×10^{-7}	6.6	4	0.0	4

	ally 2 ^e	1.1×10^4	9.9×10^{-6}	1.00×10^{10}	1.92×10^{-11}	3.95×10^{-7}	7.57×10^{-7}	8.6	5	0.0	6
	ally 3 ^e	4.8×10^4	6.8×10^{-3}	1.00×10^{10}	1.10×10^{-10}	3.95×10^{-7}	7.57×10^{-7}	29.0	0.1	0.0	2
	ally 4 ^b	6.2×10^4	1.2×10^{-3}	1.00×10^{10}	6.18×10^{-11}	3.95×10^{-7}	7.57×10^{-7}	34.5	0.5	0.0	3

k_{hyd} taken from ^aRindelaub et al., (2015); ^bWang et al., (2021); ^cHu et al., (2011); ^dDarer et al., (2011) **and** ^eJacobs et al., (2014).

Table S5. Gas-phase photolysis rate constants and lifetimes for alkyl nitrates, dinitrates and carbonyl nitrates reported from the literature.

Alkyl nitrates				
RONO ₂	Name	Global J ($\times 10^{-6} \text{ s}^{-1}$)	Global τ_{hv} (days)	Ref.
CH ₃ ONO ₂	Methyl nitrate	0.12	93	a
		0.35	33	b
	Ethyl nitrate	0.18	66	a
		0.57	20	b
		0.59	20	c
	1-Propyl nitrate	0.25	47	a
		0.75	15	c
	Isopropyl nitrate	0.68	17	a
		1.00	12	b
		0.92	13	c
	1-Butyl nitrate	0.76	15	c
	2-Butyl nitrate	0.52	22	a
	Isobutyl nitrate	0.22	53	a
		0.83	14	c
	<i>tert</i> -butyl nitrate	2.64	4	a
	1-Pentyl nitrate	0.89	13	c
	2-Pentyl nitrate	0.33	36	a
	Cyclopentyl nitrate	0.06	183	a
Dinitrates				
RONO ₂	Summer J ($\cdot 10^{-6} \text{ s}^{-1}$)	Global J · (10^{-6} s^{-1})	Global τ_{hv} (days)	Ref.
	1,2-propyl dinitrate	4.5	2.6	d
	1,2-butyl dinitrate	6.3	1.8	d
	2,3-butyl dinitrate	4.5	2.6	d
	<i>trans</i> -1-methylcyclohexyl-1,2-dinitrate	7.4	1.6	e
	<i>cis</i> -1,4-Dinitrooxy-2-butene	2.6	4.5	d
	3,4-Dinitrooxy-2-butene	1.2	10.0	d

Hydroxy nitrates				
RONO₂	Summer J (·10⁻⁶ s⁻¹)	Global J · (10⁻⁶ s⁻¹)	Global τ_{hv} (days)	Ref.
	1-Nitrooxyethanol	0.005	2400	^a
	<i>trans</i> -2-Hydroxy-cyclopentyl-1-nitrate	0	∞	^e
Carbonyl nitrates				
RONO₂	Summer J (·10⁻⁶ s⁻¹)	Global J · (10⁻⁶ s⁻¹)	Global τ_{hv} (hours)	Ref.
	α-Nitrooxyacetone	11 15	24 19	^a ^d
	1-Nitrooxy-2-butanone	7.6	37	^d
	3-Nitrooxy-2-butanone	22	13	^d
	Methylvinylketone nitrate	25	11	^f
	Methylvinylketone nitrate'	15	19	^f
	2-Oxo-cyclohexyl-1-nitrate	1	199	^e
	Ethanal nitrate	61	5	^f
	Methacrolein nitrate	149	2	^f
	4,1-Nitrooxy enal	295	1	^f

^aRoberts and Fajer, (1989). ^bTalukdar et al., (1997). ^cClemitshaw et al., (1997). ^dBarnes et al., (1993).

^eWängberg et al., (1996) ^fMüller et al., (2014).

References

- Abeleira, A., Sive, B., Swarthout, R. F., Fischer, E. V., Zhou, Y., and Farmer, D. K.: Seasonality, sources and sinks of C1-C5 alkyl nitrates in the Colorado Front Range, *Elementa*, 6, <https://doi.org/10.1525/ELEMENTA.299/112816>, 2018.
- Barnes, I., Becker, K. H., and Zhu, T.: Near UV absorption spectra and photolysis products of difunctional organic nitrates: Possible importance as NO_x reservoirs, *J Atmos Chem*, 17, 353–373, <https://doi.org/10.1007/BF00696854>, 1993.
- Bianco, A., Passananti, M., Brigante, M., and Mailhot, G.: Photochemistry of the cloud aqueous phase: A review, <https://doi.org/10.3390/molecules25020423>, 20 January 2020.
- Brimblecombe, P. and Dawson, G. A.: Wet removal of highly soluble gases, *Journal of Atmospheric Chemistry* 1984 2:1, 2, 95–107, <https://doi.org/10.1007/BF00127265>, 1984.
- Clemmshaw, K. C., Williams, J., Rattigan, O. v., Shallcross, D. E., Law, K. S., and Anthony Cox, R.: Gas-phase ultraviolet absorption cross-sections and atmospheric lifetimes of several C2-C5 alkyl nitrates, *J Photochem Photobiol A Chem*, 102, 117–126, [https://doi.org/10.1016/S1010-6030\(96\)04458-9](https://doi.org/10.1016/S1010-6030(96)04458-9), 1997.
- Darer, A. I., Cole-Filipiak, N. C., O'Connor, A. E., and Elrod, M. J.: Formation and stability of atmospherically relevant isoprene-derived organosulfates and organonitrates, *Environ Sci Technol*, 45, 1895–1902, <https://doi.org/10.1021/es103797z>, 2011.
- Fischer, M. and Warneck, P.: Photodecomposition of nitrite and undissociated nitrous acid in aqueous solution, *Journal of Physical Chemistry*, 100, 18749–18756, <https://doi.org/10.1021/jp961692+>, 1996.
- González-Sánchez, J. M., Brun, N., Wu, J., Morin, J., Temime-Roussel, B., Ravier, S., Mouchel-Vallon, C., Clément, J.-L., and Monod, A.: On the importance of atmospheric loss of organic nitrates by aqueous-phase ·OH-oxidation, *Atmos Chem Phys*, 21, 4915–4937, <https://doi.org/10.5194/acp-2020-684>, 2021.
- Herrmann, H.: On the photolysis of simple anions and neutral molecules as sources of O[•]-OH, SO_x[•]- and Cl in aqueous solution, <https://doi.org/10.1039/b618565g>, 23 July 2007.
- Herrmann, H., Schaefer, T., Tilgner, A., Styler, S. A., Weller, C., Teich, M., and Otto, T.: Tropospheric Aqueous-Phase Chemistry: Kinetics, Mechanisms, and Its Coupling to a Changing Gas Phase, *Chem Rev*, 115, 4259–4334, <https://doi.org/10.1021/cr500447k>, 2015.
- Hu, K. S., Darer, A. I., and Elrod, M. J.: Thermodynamics and kinetics of the hydrolysis of atmospherically relevant organonitrates and organosulfates, *Atmos Chem Phys*, 11, 8307–8320, <https://doi.org/10.5194/acp-11-8307-2011>, 2011.
- Jacobs, M. I., Burke, W. J., and Elrod, M. J.: Kinetics of the reactions of isoprene-derived hydroxynitrates: Gas phase epoxide formation and solution phase hydrolysis, *Atmos Chem Phys*, 14, 8933–8946, <https://doi.org/10.5194/acp-14-8933-2014>, 2014.
- Jenkin, M. E., Valorso, R., Aumont, B., Rickard, A. R., and Wallington, T. J.: Estimation of rate coefficients and branching ratios for gas-phase reactions of OH with aliphatic organic compounds for use in automated mechanism construction, *Atmos Chem Phys*, 18, 9297–9328, <https://doi.org/10.5194/acp-18-9297-2018>, 2018.
- Müller, J. F., Peeters, J., and Stavrou, T.: Fast photolysis of carbonyl nitrates from isoprene, *Atmos Chem Phys*, 14, 2497–2508, <https://doi.org/10.5194/acp-14-2497-2014>, 2014.

Nguyen, T. B., Crounse, J. D., Teng, A. P., Clair, J. M. S., Paulot, F., Wolfe, G. M., and Wennberg, P. O.: Rapid deposition of oxidized biogenic compounds to a temperate forest, *Proc Natl Acad Sci U S A*, 112, E392–E401, <https://doi.org/10.1073/pnas.1418702112>, 2015.

Poskrebyshev, G. A., Neta, P., and Huie, R. E.: Temperature Dependence of the Acid Dissociation Constant of the Hydroxyl Radical, *J Phys Chem A*, 106, 11488–11491, <https://doi.org/10.1021/jp020239x>, 2002.

Raventos-Duran, T., Camredon, M., Valorso, R., Mouchel-Vallon, C., and Aumont, B.: Structure-activity relationships to estimate the effective Henry’s law constants of organics of atmospheric interest, *Atmos Chem Phys*, 10, 7643–7654, <https://doi.org/10.5194/acp-10-7643-2010>, 2010.

Rindelaub, J. D., McAvey, K. M., and Shepson, P. B.: The photochemical production of organic nitrates from α -pinene and loss via acid-dependent particle phase hydrolysis, *Atmos Environ*, 100, 193–201, <https://doi.org/10.1016/j.atmosenv.2014.11.010>, 2015.

Roberts, J. M. and Fajer, R. W.: UV Absorption Cross Sections of Organic Nitrates of Potential Atmospheric Importance and Estimation of Atmospheric Lifetimes, *Environ Sci Technol*, 23, 945–951, <https://doi.org/10.1021/es00066a003>, 1989.

Sander, R.: Compilation of Henry’s law constants (version 4.0) for water as solvent, *Atmos Chem Phys*, 15, 4399–4981, <https://doi.org/10.5194/acp-15-4399-2015>, 2015.

Talukdar, R. K., Burkholder, J. B., Hunter, M., Gilles, M. K., Roberts, J. M., and Ravishankara, A. R.: Atmospheric fate of several alkyl nitrates: Part 2. UV absorption cross-sections and photodissociation quantum yields, *Journal of the Chemical Society - Faraday Transactions*, 93, 2797–2805, <https://doi.org/10.1039/a701781b>, 1997.

Wang, Y., Piletic, I. R., Takeuchi, M., Xu, T., France, S., and Ng, N. L.: Synthesis and Hydrolysis of Atmospherically Relevant Monoterpene-Derived Organic Nitrates, *Environ Sci Technol*, 55, 14595–14606, <https://doi.org/10.1021/acs.est.1c05310>, 2021.

Wängberg, I., Barnes, I., and Becker, K. H.: Atmospheric chemistry of bifunctional cycloalkyl nitrates, *Chem Phys Lett*, 261, 138–144, [https://doi.org/10.1016/0009-2614\(96\)00857-3](https://doi.org/10.1016/0009-2614(96)00857-3), 1996.